

# Magnetic Sensors and Their Applications

James Lenz and Alan S. Edelstein

**Abstract**—Magnetic sensors can be classified according to whether they measure the total magnetic field or the vector components of the magnetic field. The techniques used to produce both types of magnetic sensors encompass many aspects of physics and electronics. Here, we describe and compare most of the common technologies used for magnetic field sensing. These include search coil, fluxgate, optically pumped, nuclear precession, SQUID, Hall-effect, anisotropic magnetoresistance, giant magnetoresistance, magnetic tunnel junctions, giant magnetoimpedance, magnetostrictive/piezoelectric composites, magnetodiode, magnetotransistor, fiber optic, magnetooptic, and microelectromechanical systems-based magnetic sensors. The usage of these sensors in relation to working with or around Earth's magnetic field is also presented.

**Index Terms**—Anisotropic magnetoresistance, fluxgate, giant magnetoresistance, magnetic, magnetic tunnel junctions, magnetoresistance, microelectromechanical systems (MEMS), optically pumped, sensor, spin valves, superconducting quantum interference device (SQUID).

## I. INTRODUCTION TO MAGNETIC SENSOR TECHNOLOGIES

THIS paper discusses and reviews magnetic sensors and their applications. Magnetic sensors have assisted mankind in analyzing and controlling thousands of functions for many decades. Computers have nearly unlimited memory through the use of magnetic sensors in magnetic storage disks and tape drives. Airplanes fly with higher safety standards because of the high reliability of noncontact switching with magnetic sensors. Automobiles use magnetic sensors to determine position in several places such as the engine crank shaft and wheel braking. Factories have higher productivity because of the stability and low cost of magnetic sensors. The subject has been reviewed previously [1]–[3].

There are many ways to sense magnetic fields, most of them based on the intimate connection between magnetic and electric phenomena. In the first half of this paper, the more popular sensor technologies will be described with examples of products. In the second half, the major applications of magnetic sensors are discussed in relation to four categories: measuring fields stronger than the Earth's field, measuring perturbations in the Earth's field, measuring small changes or gradients in generated or induced magnetic fields, and medical/biological applications. A common theme among all applications is that magnetic sensors provide a very rugged, reliable, and maintenance-free technology.

Manuscript received October 1, 2004; revised December 6, 2005. This work was supported by the ONR and DARPA. The associate editor coordinating the review of this paper and approving it for publication was Dr. Usha Varshney.

J. Lenz is with the University of Minnesota, Minneapolis, MN 55454 USA (e-mail: lenzjamese@johndeere.com).

A. S. Edelstein is with the U.S. Army Research Laboratory, Adelphi, MD 20783-1197 USA (e-mail: edelstein@arl.army.mil).

Digital Object Identifier 10.1109/JSEN.2006.874493

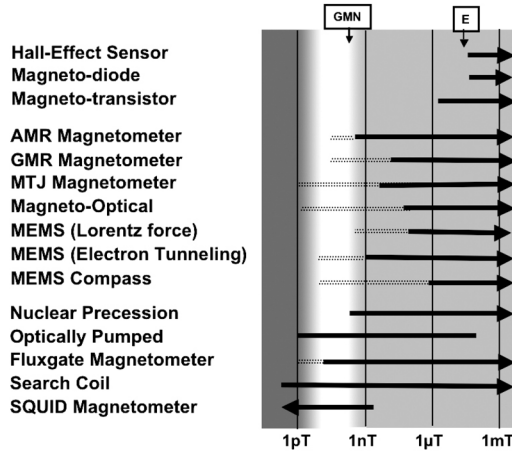


Fig. 1. Estimate of sensitivity of different magnetic sensors. The symbols E and GMN are used to indicate the strength of the Earth's magnetic field and geomagnetic noise, respectively.

Magnetic sensing techniques exploit a broad range of ideas and phenomena from the fields of physics and material science. Most of the more common magnetic sensor technologies are listed in Fig. 1, which compares approximate sensitivity ranges. In Fig. 1, the symbols E and GMN are used to indicate the strength of the Earth's magnetic field and geomagnetic noise, respectively. Because of the large magnitude of the Earth's magnetic field, sensitive sensors must either have a large dynamic range or use a coil to decrease the field at the position of the sensor. Geomagnetic noise is spatially correlated over distances of the order of kilometers because it arises from sources that are spatially large, such as currents in the ionosphere that are driven by tidal forces and winds [4]. Thus, by taking the difference between the readings of two or more spatially separated sensors it is possible to measure magnetic field changes smaller than the geomagnetic noise. The geomagnetic noise is about 0.1 nT at low frequencies and has a  $1/f$ -like frequency spectrum. It is important to note that the sensitivity range for each type of sensor is influenced by the readout electronics. There are many other factors, particularly frequency response, size, and power, that affect which sensor is best suited for an application. Another important consideration is whether the magnetometer measures just the magnitude of the field or measures each of its vector components. One might think that since vector magnetometers provide additional information, vector magnetometers are always better than magnetometers that measure only the magnitude of the field. The latter are often called scalar or total field magnetometers.

For some applications, scalar magnetometers are much better than vector magnetometers. Consider using a magnetometer on a moving vehicle and trying to detect small changes due to ferromagnetic objects. Rotational vibrations due to the vehicle's

motion will generate changes in the vector components of the Earth's field detected by a vector magnetometer that are difficult to separate from the signal. These changes in the components are often much bigger than the changes due to the ferromagnetic objects. Accurately computing the total field from the vector components is difficult because the sensitivities of the three vector magnetometers must be identical and their axes exactly perpendicular. Thus, in this application a total field magnetometer is much better than a vector field magnetometer.

## II. MAGNETIC SENSORS

This section discusses the different kinds of magnetic sensors. It is divided into two parts: one that discusses vector magnetometers and the other discusses scalar magnetometers. Before further discussion, it is worth comparing some of the units used to describe the magnetic field strength. The units for magnetic field in air are:  $1 \text{ T} = 10^4 \text{ Oe} = 10^4 \text{ G} = 10^9 \text{ nT} = 10^9 \text{ gamma} = 10^{12} \text{ pT} = 10^{15} \text{ fT} = 1/4\pi \times 10^7 \text{ amper-turns/meter}$ . Note we are not distinguishing here between H and B.

### A. Vector Magnetometers

There are several problems that affect most vector sensors. First, nearly all vector magnetometers suffer from noise [5], especially  $1/f$  noise [6]. One attempt at mitigating the effect of  $1/f$  noise is the work being done on a device, the MEMS flux concentrator [7], [8], which will shift the operating frequency above the range where  $1/f$  noise dominates. The device is discussed further in Section II-A12. Another major problem with vector magnetometers, discussed earlier, is that they are affected by rotational vibrations.

1) *Search-Coil Magnetometer*: The principle behind the search-coil magnetometer is Faraday's law of induction. If the magnetic flux through a coiled conductor changes, a voltage proportional to the rate of change of the flux is generated between its leads. The flux through the coil will change if the coil is in a magnetic field that varies with time, if the coil is rotated in a uniform field, or if the coil is moved through a nonuniform field. Typically, a rod of a ferromagnetic material with a high magnetic permeability is inserted inside the coil to "gather" the surrounding magnetic field and increase the flux density (the permeability of a material is a measure of the extent to which it modifies the magnetic flux in the material).

The signal detected by a search-coil magnetometer depends on the permeability of the core material, the area of the coil, the number of turns, and the rate of change of the magnetic flux through the coil. The frequency response of the sensor may be limited by the ratio of the coil's inductance to its resistance, which determines the time it takes the induced current to dissipate when the external magnetic field is removed. The higher the inductance, the more slowly the current dissipates, and the lower the resistance, the more quickly it dissipates. In some cases, the inter-winding capacitance can also limit the frequency response. In practice, however, the voltage readout electronics can limit both the sensitivity and the frequency response of the sensor.

Sensors of this type can detect fields as weak as  $20 \text{ fT}$  ( $2 \times 10^{-5} \text{ nT}$ ), and there is no upper limit to their sensitivity range. Their useful frequency range is typically from 1 Hz to 1 MHz, the upper limit being that set by the ratio of the coil's inductance

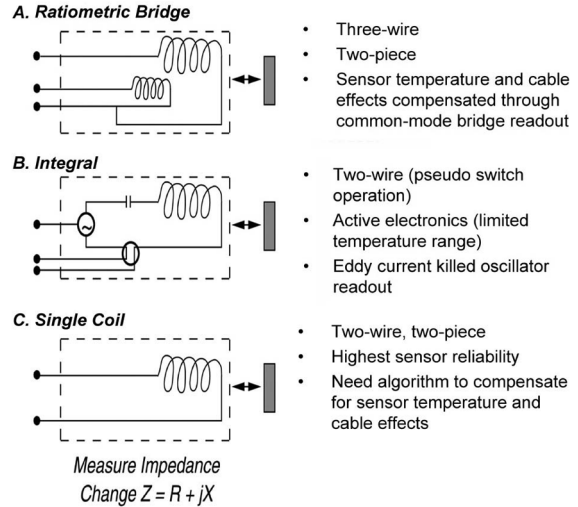
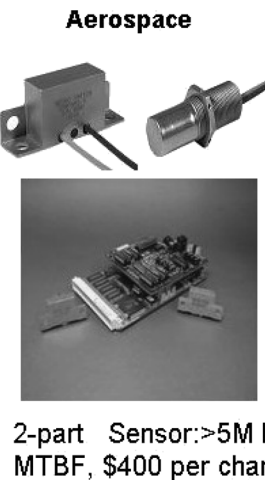


Fig. 2. Illustration of three types of proximity sensors for detecting metallic objects: (a) resonant circuit method, (b) bridge method, and (c) single-coil method.

to its resistance. The sensor's coil can be as short as 2 in or as long as 50 in. They require between 1 and 10 mW of power, all of which is consumed in the readout electronics.

In addition to this passive use, one can also operate a search coil in an active mode to construct a proximity sensor. The active-mode method involves incorporating the search coil as an inductive element in an electrical circuit. Fig. 2 illustrates three configurations for use of inductance coils to detect the presence of metallic targets. This type of sensor is commonly called a proximity switch or proximity sensor. The first method illustrated in Fig. 2(a) incorporates a balanced inductive bridge where an inductance change in one leg of the bridge produces an out-of-balance voltage in the circuit. The second circuit design, Fig. 2(b), incorporates a resonant circuit where a change in inductance results in a change in the circuit's resonant frequency. This circuit is sometimes referred to as an eddy-killed oscillator, since conductive materials near the active coil will have eddy currents induced, which will produce a mutual inductance change in the circuit. Ferrite cores are often used in this approach because they can be designed with the coil to offer a temperature insensitive impedance. The third approach shown in Fig. 2(c) uses a single coil in the sensor and the remainder of the electronics is connected remotely. This is a challenging implementation because the readout electronics must compensate the inductive readout for temperature and cable effects. Examples of various products using active search coils are shown in Fig. 3. This type of sensor is primarily used in harsh environments where high reliability sensing can be afforded such as on aircraft door checks or for indicating the position of slats and landing gear.

2) *Fluxgate Magnetometer*: The fluxgate magnetometer [9] illustrated in Fig. 4 consists of a ferromagnetic material wound with two coils, a drive and a sense coil. It exploits magnetic induction together with the fact that all ferromagnetic material becomes saturated at high fields. This saturation can be seen in the hysteresis loops shown on the right side of Fig. 4. When a sufficiently large sinusoidal current is applied to the drive coil, the core reaches its saturation magnetization once each half-cycle.



1-part Integral Electronics, Smart Interface, \$40 per channel

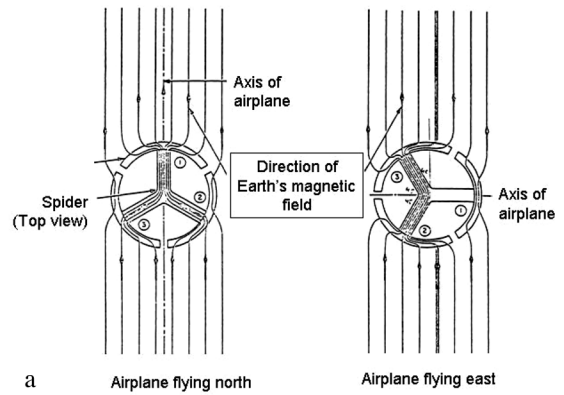


Fig. 3. Examples of proximity sensors.

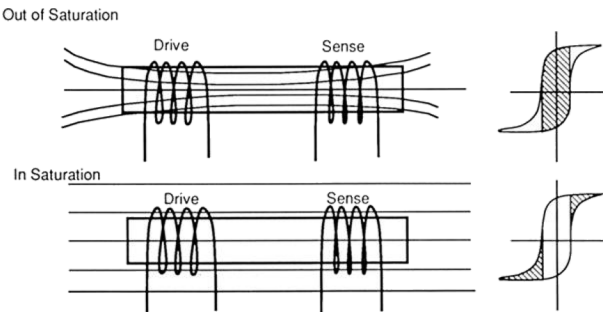


Fig. 4. Illustration of the operating principles of fluxgate magnetometers. The output signal becomes modulated by driving the soft magnetic core into and out of saturation. The shaded regions indicate the regions of operation.

As the core is driven into saturation, the reluctance of the core to the external magnetic field being measured increases, thus making it less attractive for any additional magnetic field to pass through the core. This change is detected by the sense coil. When the core comes out of saturation by reducing the current in the drive coil, the external magnetic field is again attracted to the core, which is again detected by the sense second coil. Thus, alternate attraction and lack of attraction causes the magnetic lines of flux to cut the sense coil. The voltage output from the sense coil consists of even-numbered harmonics of the excitation frequency. For readout, the second harmonic is extracted and rectified. The voltage associated with this harmonic is proportional to the external magnetic field.

The sensitivity of this sensor depends on the shape of the hysteresis curve. For maximum sensitivity, the magnetic field-magnetic induction ( $B$ - $H$ ) curve should be square, because this produces the highest induced electromotive force (emf) for a given value of the magnetic field. For minimum power consumption, the core material should have low coercivity and saturation values. The sensitivity range is from  $10^{-2}$  to  $10^7$  nT. The frequency response of the sensor is limited by the excitation field and the response time of the ferromagnetic material. The upper limit on the frequency is about 10 kHz. Fluxgate magnetometers resemble the search-coil magnetometers in size, but they



Fig. 5. Fluxgates used as compasses. (a) Illustration showing how the signals of a three axis fluxgate change as the axis are rotated. (b) Aircraft compass system that uses a three axis fluxgate.

consume roughly five times as much power. The major advantage of fluxgate magnetometers over search coils is their ability to precisely measure direct current (dc) fields.

Many versions of fluxgate magnetometers have been developed. Most of these achieve lower power consumption by operating the sensor on a minor hysteresis loop, thus not driving the core from saturation to saturation. These minor-loop fluxgate magnetometers are much more sensitive to the drive and readout electronics than the major-loop versions, whose performance is governed mostly by the core material's properties.

Fig. 5 illustrates how a three-arm version of a fluxgate magnetometer can be used to create a simple three-voltage readout for determining an accurate compass heading. Also shown is an aircraft compass system that has been used for more than 30 years. A typical system for aircraft heading offers as good as  $0.1^\circ$  accuracies. By appropriately ratioing the sensed field in each of the three spiders, the angle of Earth's magnetic field with respect to the spider is determined without ambiguity. This three-spider flux gate is gimbaled so that the sensor's sensitivity plane is always horizontal.

### 3) Superconductor Magnetometers:

a) *SQUID* sensors: The most sensitive of all instruments for measuring a magnetic field at low frequencies (<1 Hz) is the superconducting quantum interference device (SQUID) [10], [11] illustrated in Fig. 6. It is based on the remarkable interactions of electric currents and magnetic fields observed when certain materials are cooled below a superconducting transition temperature. At this temperature, the materials become superconductors and they lose all resistance to the flow of electricity.

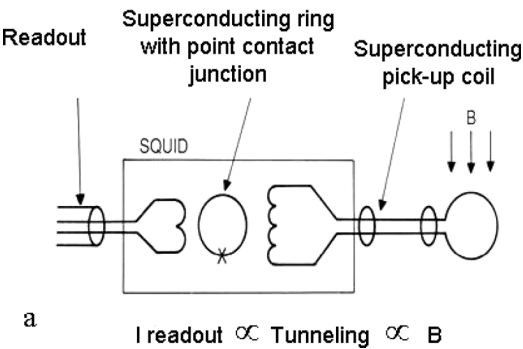


Fig. 6. Schematic of SQUID.

If a line of magnetic flux becomes threaded through a ring made of a superconducting material, a current is induced in the ring; in the absence of any further disturbances the current would continue flowing forever. The magnitude of the induced current is an exquisitely sensitive indicator of the flux density. It turns out that the flux through the ring is quantized [12], [13] and that the flux can only take on values that are integer multiples of a basic flux quanta  $\phi_0 = hc/2e \approx 2 \times 10^{-7}$  gauss cm<sup>2</sup>.

How is the current in the superconducting ring to be measured? Josephson, who was then a graduate student at the University of Cambridge, provided [14] the key to the answer in 1962. Josephson considered what would happen in a superconducting ring interrupted by a “weak-link,” either a thin layer of insulator or an area where the superconductor itself narrows to a very small cross section. He predicted that a supercurrent can flow through the weak link and that this supercurrent would be an oscillating function of the magnetic field intensity in the weak link. The periodic variations in the current have the same pattern as the interference fringes produced by the diffraction of light and are related to the flux quantization described above.

In a SQUID, the periodic variations are exploited to measure the current in the superconducting ring and, hence, the ambient magnetic field. Typically, the ring is inductively coupled to a radio-frequency circuit that both supplies a known bias field and serves as the detector output. Changes in the ring current alter the resonant frequency of the circuit; as a result, the output signal changes periodically as the field varies. Changes in the field can be measured simply by counting the peaks and valleys much as one would count fringes in an interference pattern. Alternatively, a feedback loop can be employed to lock the radio-frequency circuit onto a single peak, continually adjusting the bias field to compensate for changes in the external field. The feedback current is then a measure of the ambient field. One can also form a dc SQUID by employing two Josephson junctions in the ring. When the two weak links are matched properly through design, the current in the ring has a dc response to the flux going through it.

The superconducting ring in a SQUID is typically a toroid a few millimeters in diameter made of a metal such as lead or niobium. The weak link is a narrow constriction in the superconductor or a point-contact junction. Sensitivity is improved by coupling the ring to a larger superconducting loop or coil (without a weak link), which effectively serves as a magnetic “antenna” or dc search coil, gathering flux over an area of several

square centimeters. Using superconducting properties, one can form a dc transformer between the sense loop and the SQUID readout. The SQUID ring essentially serves as a very precise ammeter for measuring the current in the pickup coil. Thus, the device has three superconducting components: the SQUID ring itself, the radio-frequency coil, and the large antenna loop. All three must be cooled to a superconducting state.

The sensitivity of SQUIDs is limited by the magnetic field noise and for commercial DC SQUIDs this noise [15] is of order 10 fT or  $10^{-5}$  nT. The ability to set a null level by adjusting the bias field in the radio-frequency circuit makes the device particularly useful for differential field measurements. For example, if the null level is set to the average terrestrial magnetic field, the instrument will readily detect anomalies in the field. The SQUID itself can be quite small, but the need for liquid-helium coolant makes the complete instrument rather bulky and heavy. The power consumption of several watts is due almost entirely to the radio-frequency electronics. The sensing loop can be configured to be sensitive to a gradient in the measuring field by cross-connecting two parallel turns. Because the sense loop is superconducting, it has a dc response to magnetic fields. By orienting the coils properly, the gradient of a component of the external field in any direction can be sensed (i.e.,  $\delta B_x/\delta x, \delta B_x/\delta y, \delta B_x/\delta z, \delta B_y/\delta x$ , etc.). The ability to fabricate a high-sensitivity gradiometer that can measure any of these partial derivatives is a unique feature of this technology over other magnetic sensor schemes.

A new family of materials that exhibit superconductive properties in the 30 K region was discovered, [16] and later work [17] found superconductors with superconducting transition temperatures above liquid-nitrogen (77 K) temperature. The potential for higher temperature SQUID magnetometers appears available. The most obvious benefit of the high-temperature superconductors will be a thinner insulation jacket between the sense loops and the magnetic field being mapped. However, the higher temperature operation may also lead to a reduction in the high sensitivity achieved with liquid-helium operation (4 K) for the following reasons: 1) higher Johnson noise in the readout electronics, 2) lower rigidity between gradiometer coils, and 3) higher thermal gradients and variations across the superconductors. To date, magnetometers [10] built using these new superconductors, called high T<sub>c</sub> temperature superconductors (HTSC), do not have as good a sensitivity as those built with low temperature superconductors.

The high sensitivity of SQUIDs allow them to be used in astronomy [18], geological [19], and medical applications [20]. SQUIDs also provide one of the more promising approaches to quantum computing [21], [22]. A digital SQUID sensor based on single-flux-quantum with a large slew rate has been developed [23].

*b) Using the Meissner effect:* Induced currents in superconductors exclude magnetic fields below a critical field. This effect is called the Meissner effect [24]. The Meissner effect has been used in a superconducting flux-to-field transformer to construct a magnetometer [25]. They use a superconducting loop perpendicular to the field direction with a width that is 0.7 times the radius and that has a micron size constriction. The shielding current, which is greatly enhanced in the constriction, generates

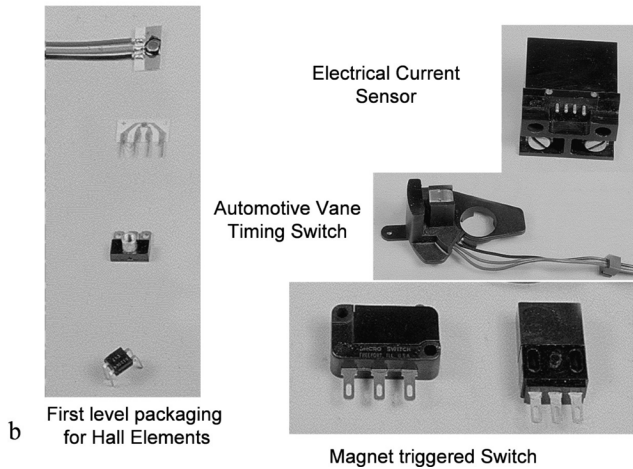
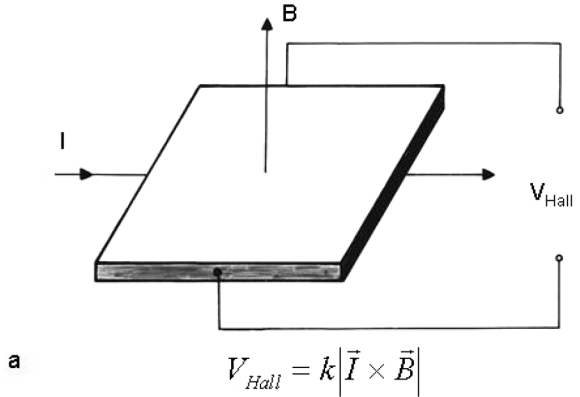


Fig. 7. (a) Schematic of Hall effect sensors. (b) examples of Hall effect products.

a field that is measured by a GMR sensor located near the constriction. The field is sensed by a low-noise giant magnetoresistance sensor. The small size prototype can be used at 77 K and is capable of measuring 32 ft or  $3.2 \times 10^{-5}$  nT at 4 K.

4) *Hall Effect Sensor*: The Hall effect sensor [26] is a widely used, low cost sensor whose operation is illustrated in Fig. 7(a). The sensor exploits a physical phenomenon discovered by Edwin H. Hall more than 100 years ago. He found that a voltage difference appears across a thin rectangle of gold placed in a strong magnetic field perpendicular to the plane of the rectangle when an electric current is sent along its length. An electron moving through a magnetic field experiences a force, known as the Lorentz force, that is perpendicular both to its direction of motion and to the direction of the field. It is the response to this force that creates the Hall voltage.

The Hall effect is very small in metallic conductors, but a semiconductor gives a much larger effect. Since there are fewer conduction electrons in a semiconductor, if the total current through it is the same as that through a metal, the electrons in the semiconductor must have a much higher drift velocity than those in the metal. The faster the electrons are moving, the stronger the force they experience and the greater the Hall voltage produced at equilibrium. Inexpensive Hall effect sensors are generally made of silicon. More sensitive sensors can be made of the III-V semiconductors, which have higher electron mobilities than silicon. Most commercially available Hall effect mag-

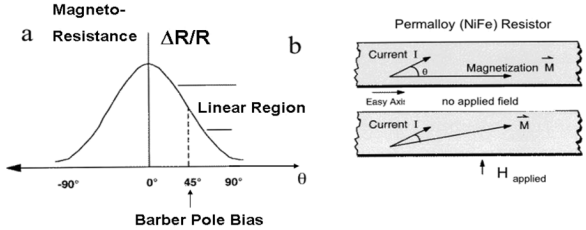


Fig. 8. AMR sensor (a) resistance versus angle  $\theta$  between the magnetization and the direction of current flow; (b) change in  $\theta$  due to the application of a magnetic field.

netometers have sensing elements made of the III-V semiconductor indium antimonide.

The silicon devices have a sensitivity range of 10 to 1000 G or  $10^6$  to  $10^8$  nT, and the indium antimonide sensors extend the lower limit to  $10^{-3}$  G or  $10^2$  nT. Hall effect sensors can measure either a constant or a varying field; the upper frequency limit is about 1 MHz. They are light and occupy about 0.1 in<sup>2</sup>. Their power requirement is between 0.1 and 0.2 W, and they can be operated over an extremely wide temperature range limited only by packaging and lead attachment to the semiconductor. Hall effect devices, shown in Fig. 7(b), have found hundreds of uses in low cost position sensor applications.

5) *Magnetoresistive Magnetometers*: Magnetoresistance magnetometers [27] use a change in resistance  $\Delta R$  caused by an external magnetic field  $H$ . Magnetoresistance magnetometers are very attractive for low cost applications because they are simply energized by applying a constant current and the output voltage is a measure of the magnetic field. Mapps has written a review [28] of magnetoresistance sensors that includes a discussion of the effect of Barkhausen noise. Values for the magnetoresistance  $MR$  are given as  $\Delta R/R$  where  $R$  is the  $H = 0$  value of the resistance. The value for  $MR$  is usually expressed as the percentage change in the resistance per Oe or in the voltage change out per volts in per Oe. Usually  $\Delta R/R$  is small. Thus, the DC voltage change is small and one must use a bridge circuit and other methods to minimize the DC offset. Modulation techniques such as that of the MEMS flux concentrator [7] are useful for eliminating the DC offset. Several different kinds of magnetoresistance sensors that are based on different mechanisms are discussed in the following subsections.

a) *Anisotropic magnetoresistance, AMR, sensors*: Some materials, such as permalloy (an alloy containing about 80% nickel and 20% iron), exhibit anisotropic magnetoresistance. In such materials, the resistance depends on the angle between the magnetization and direction of current flow [29]. These sensors are called anisotropic magnetoresistance or AMR sensors. In a field, the magnetization will rotate toward the direction of the magnetic field. The angle through which it rotates depends on the magnitude of the external magnetic field. The resistance of permalloy decreases as the direction of magnetization rotates away from the direction in which the current flows and is lowest when the magnetization is perpendicular to the direction of current flow. The resistance changes roughly as the square of the cosine of the angle between the magnetization and the direction of current flow. Fig. 8 illustrates the magnetoresistive effect. Though the magnetization rotates in the direction of an applied

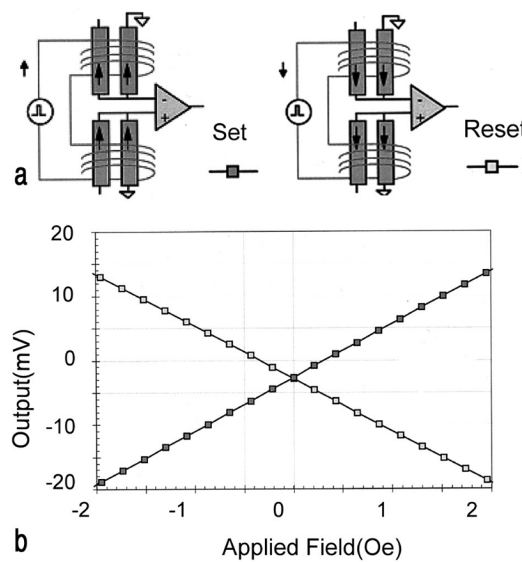


Fig. 9. Figure illustrating set and reset operation of anisotropic magnetoresistive sensor. (a) Direction of current flow in coils that set and reset the direction of the magnetization of the cores. (b) Output voltage as a function of the field when the coil operates in the set and reset mode.

magnetic field, it generally does not end up pointing in the same direction as the field because its direction is determined by several competing factors. One factor is the easy axis, the direction along which the magnetization in a circular film prefers to lie, which is determined by the magnetic field present during deposition of the film. Another factor is the shape of the film, which in the case of a long, thin film, tends to keep the magnetization in the plane of the film and tends to make it point along the length of the film. Further, there is a crystalline anisotropy that tends to make the magnetization align along certain directions in the crystal.

Permalloy is the most common material for AMR sensors because it has a relatively large magnetoresistance and because its characteristics are compatible with the fabrication techniques employed to make silicon integrated circuits such as a zero coefficient of magnetostriction. The magnetoresistance [30] of permalloy is less than 4%. As shown in Fig. 9(a), an integrated sensor normally consists of four Permalloy resistors sputter-deposited on a silicon substrate. The four resistors form a two-legged current path called a bridge. A voltage develops between the two legs of the bridge if the resistance of one leg is different from that of the other. Having a long path design allows for a high bridge resistance and minimizes the power requirement of the sensor. An offset voltage in a magnetoresistive bridge can arise from the inherent resistance of the four resistors that are not precisely matched. In designing anisotropic magnetoresistance bridges, one can use a method that greatly reduced the offset from mismatches in the four resistors. This set/reset method is illustrated in Fig. 9(b). By changing the direction of the magnetization in the thin film the bridge output changes sign. Fig. 9(b) shows the bridge voltage produced from an applied field when the magnetization is set in one direction and then reversed (reset). This setting of the magnetization is done by applying a strong magnetic field for a short time along

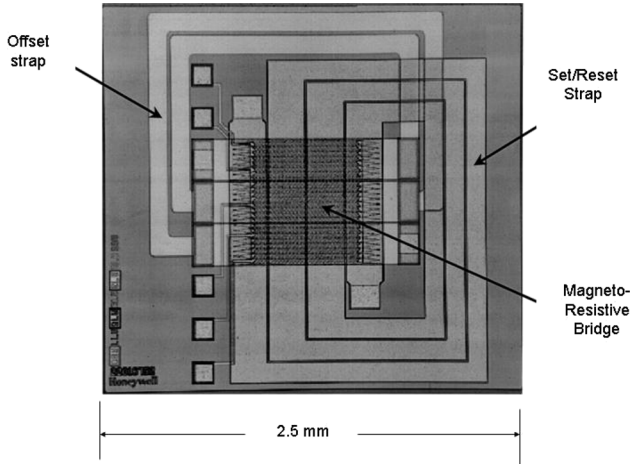


Fig. 10. Picture showing the die configuration of an AMR sensor. Included in the photograph are the four resistors of the bridge, each consisting of a serpentine path and two coils—one for creating the set/reset field pulses and the other for producing a feedback field.

the direction desired. By subtracting the voltage reading when the sensor is in the reset mode from the voltage reading in the set mode [see Fig. 9(b)], the inherent resistance and its noise (such as temperature effects) is cancelled and resulting value represents twice the output for the applied field measurement. This symmetry in AMR sensors is accurate to parts per million or better depending on the quality of the film.

Fig. 10 shows a photograph of the four resistors, each consisting of a serpentine path. Also shown are two coils, one for creating the set/reset field pulses and the other for producing a feedback field so the bridge can be operated in a null field. The bridge voltage readout electronics can also be fabricated on the same chip as the resistors, and additional temperature-compensating circuitry can also be included on the chip. Each resistor is biased so that its direction of magnetization is rotated to bring it into a region where the change in resistance that results from a change in the magnetic field is linear and relatively large. This can be done by sputtering a thin film of cobalt over the resistors and magnetizing the cobalt or, more commonly, by adding shorting paths on the permalloy strips that look like a barber pole causing the current to run at 45° with respect to the direction of the magnetization.

The magnetoresistive sensors have a sensitivity range of  $10^{-2}$  to 50 G or  $10^3$  to  $5 \times 10^6$  nT with open-loop readout electronics. With closed-loop feedback readout electronic methods, the minimum detectable field can be reduced to 0.1 nT for limited bandwidths. With open-loop readout electronics, these sensors have an extremely wide dynamic range from dc to nearly 1 GHz. These sensors are light, small, require between 0.1 and 0.5 mW of power, and can be operated at temperatures between  $-55^{\circ}\text{C}$  and  $200^{\circ}\text{C}$ .

b) *Giant magnetoresistance GMR sensors:* Larger changes in magnetoresistance were observed [31], [32] in planer structures of metals. The effect was named giant magnetoresistance or GMR. In its simplest form, GMR is achieved by using a four layer structure that consists of two thin ferromagnets separated by a conductor. The fourth layer is an antiferromagnet that is used to pin (inhibit the rotation) the

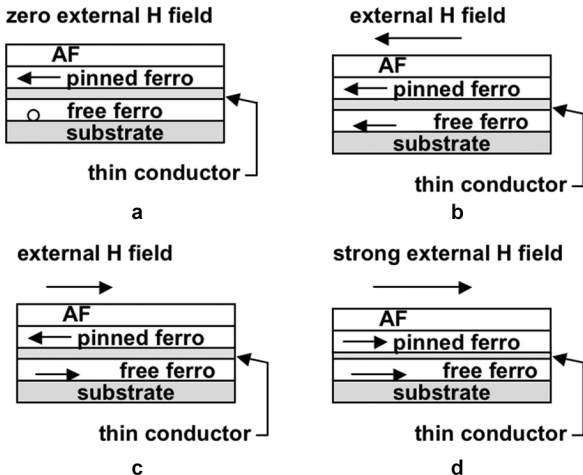


Fig. 11. Orientation of the magnetization of the ferromagnetic layers in a GMR spin valve for different external fields  $H$ . (a)  $H = 0$ , the magnetization of the free ferromagnetic layer is perpendicular to the magnetization of pinned ferromagnet,  $R = R(0)$ . (b) Low resistive state,  $H$  parallel to the magnetization of the pinned ferromagnet,  $R < R(0)$ . (c) High resistive state,  $H$  directed opposite to the magnetization of the pinned ferromagnet,  $R > R(0)$ . (d)  $H$  large enough to unpin the pinned ferromagnet,  $R < R(0)$ .

magnetization of one of the ferromagnetic layers. The ferromagnet layer that is being pinned is between the conductor and the antiferromagnet. The pinned ferromagnet is called the hard ferromagnet and the unpinned ferromagnet is called the soft ferromagnet. This structure is called a spin valve [33]. Electrons can travel more easily either parallel to the layers or perpendicular to the layers if the magnetizations of the two ferromagnets are parallel to one another. The reason for this is that when the magnetizations are parallel, electrons suffer less scattering in going from an electronic band structure state in one of the ferromagnets into a similar or identical electronic band structure state in the other ferromagnet. The difference in resistivity between the case when the magnetizations are parallel to when they are antiparallel can be as large as 12.8% at room temperature [34]. To optimize the effect the layers must be a very thin, i.e. about a nanometer thick. For the low field response of the sensor to be a linear function of the field, it is necessary that the soft ferromagnetic have its easy axis of magnetization in zero field perpendicular to the magnetization of the pinned ferromagnet. The zero field orientation of the two magnetizations is depicted in Fig. 11(a). The resistance is measured either in the plane of the ferromagnetics or perpendicular to this plane.

It is possible to eliminate the antiferromagnetic pinning layer by adjusting the thickness of the nonferromagnetic conducting layer so that the two ferromagnets are coupled antiferromagnetically [35]. In this case, the resistance is maximum at  $H = 0$ . A difficulty with this approach is that the sensor is insensitive and nonlinear near  $H = 0$ .

The basic three or four layer structure can be repeated to create a multilayer geometry. This multilayer geometry increases the percentage resistance change because it increases the probability of spin flip scattering by increasing the number of interfaces where spin flip scattering occurs. In cases where the resistance can be measured perpendicular to the plane, the

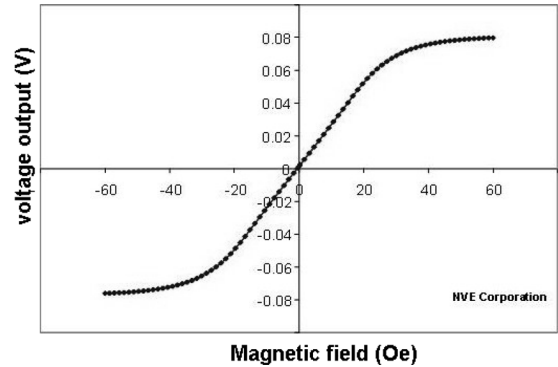


Fig. 12. Voltage output versus field for a spin valve supplied by NVE Corp.

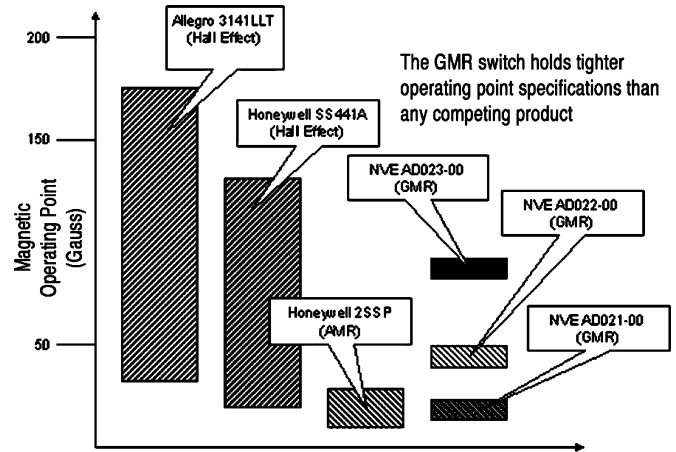


Fig. 13. Operating point error band for magnetic switches for 4.5 to 30 V, 40 °C to 70 °C. Note that the GMR switches have more reproducible switching characteristics.

multiplayer geometry provides a larger resistance and resistance change. It is very desirable that the layers should be very smooth to minimize coupling between the layers [36]. GMR sensors are used in most current computer read heads. How the directions of the magnetization of the two ferromagnetic layers change with the application of a magnetic field is illustrated in Fig. 11. Fig. 12 shows a plot of the voltage output from a spin valve versus applied field. One does not have to use any set/reset feature with spin valves, but they tend to have more  $1/f$  noise than AMR sensors. Present GMR sensors can be used in fields as small as 10 nT at 1 Hz to as large as about  $10^8$  nT. Fig. 13 shows the switching characteristics of several kinds of magnetic switches. Note the NVE GMR switches operate in a narrow reproducible band.

c) *Magnetic tunnel junction sensors:* Magnetic tunnel junctions (MTJ) or spin dependent tunneling (SDT) sensors [37], [38], first fabricated 1995, have a structure similar to the four layer structure described above in GMR sensors. Again there are two ferromagnets separated by an intervening layer, but in this case the intervening layer is an insulator. In MTJ sensors, the conduction occurs by tunneling of electrons across the insulator. The insulating layer must be very thin, about 1 nm thick and is usually  $\text{Al}_2\text{O}_3$ . One must avoid shorting the junctions either in fabricating the junction or by accidentally applying an electric field across the junction that forms a

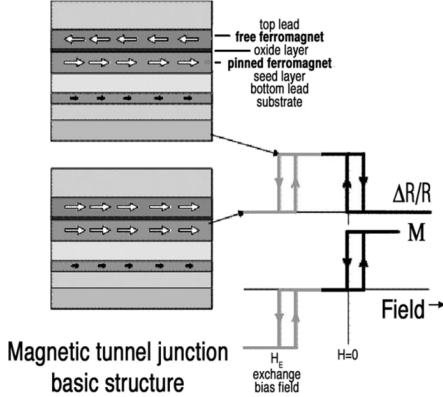


Fig. 14. MTJ sensor. In the application shown, the device is a switch. A different design must be employed if the device is to be used as a linear sensor.

pin hole or metallic bridge. Again, the layers should be very smooth to minimize coupling between the layers [36]. As was discussed above for spin valves, the magnetization of one of the ferromagnetic layers is pinned by being in contact with a layer of an antiferromagnet. Just as for GMR sensors, in order for the low field response of MTJ sensors to be a linear function of the field it is necessary that the soft ferromagnetic have its easy axis of magnetization in zero field perpendicular to the magnetization of the pinned ferromagnet. Making the magnetization of the soft ferromagnet perpendicular to the magnetization of the hard ferromagnet can be accomplished using shape anisotropy or by applying a field. The latter method usually greatly increases the power consumption of the sensor. Based on a spin-polarized tunneling model [39] the magnetoresistance ratio  $MR$  or  $\Delta R/R$  is given by

$$\Delta R/R = (R_a - R_p)/R_p = 2P_1 P_2 (1 - P_1 P_2) \quad (1)$$

where  $R_p$  and  $R_a$  are the resistances when the two ferromagnets are parallel and antiferromagnetic, respectively, and  $P_1$  and  $P_2$  are the spin polarizations of the two ferromagnets at the Fermi surface. Fig. 14 shows the structure of a MTJ sensor and how the magnetization and resistance changes as a function of magnetic field. The device shown is for a read head in a magnetic hard drive. For a sensor used to determine an arbitrary field, the change in resistance should be linear in field and the hysteresis should be zero. In January 2004,  $MR$  values as large as 70% were reported for MTJ sensors at room temperature. Roughly a year later two groups reported [40], [41]  $MR$  values of 180%–220% for MTJ sensors with MgO barriers at room temperature. The use MgO barriers was motivated by theoretical calculations [42], [43] that showed that the tunneling conductance is strongly dependent on the symmetry of the electron states of the electrodes and the evanescent states in the barrier. The theory predicted that the magnetoresistance would increase with barrier thickness.

MTJ sensors have higher magnetoresistance values and base impedance than GMR sensors. Because of their higher impedance, MTJ sensors use less power than GMR sensors. These devices often have an inherent noise that is much larger than the Johnson noise limit. Klaassen *et al.* [44] give a general discussion of noise in MTJ sensors pointing out that different

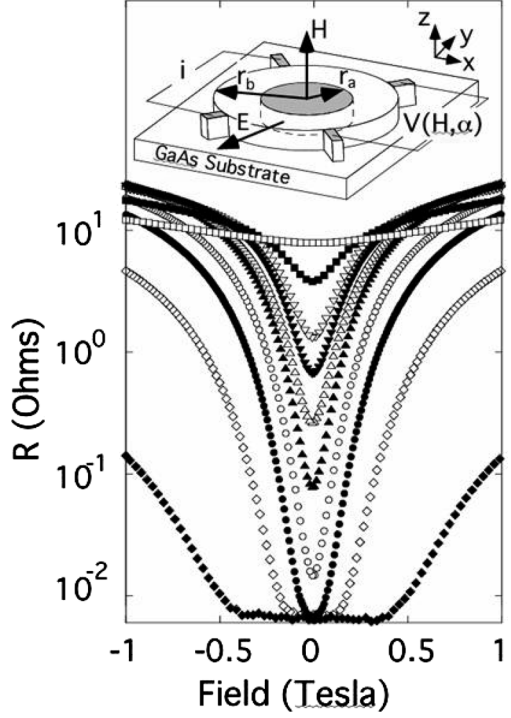


Fig. 15. Room temperature resistance as a function of field for several extraordinary magnetoresistance sensors for several values of  $r_a/r_b$ . The symbols correspond to values of  $16\alpha = 0$ ,  $\square$ ; 6,  $\blacksquare$ ; 8,  $\triangle$ ; 9,  $\tau$ ; 10,  $\Delta$ ; 11,  $\sigma$ ; 12,  $\circ$ ; 13,  $\bullet$ ; 14,  $f$ ; and 15,  $\blacklozenge$ .

noise mechanisms, such as shot noise, dominate at different bias voltages. Because of their high magnetoresistance, high impedance, and planer geometry, MTJ sensors have potential for being used as low cost, energy efficient, high sensitivity magnetic sensors. A single axis MTJ has been used to construct a two-axis magnetometer [45]. MTJs are the key element in nonvolatile random access memory (MRAM).

*d) Extraordinary magnetoresistance:* Large values of room temperature magnetoresistance have been obtained [46] by using narrow-gap semiconductors in a special geometry. The geometry is shown in Fig. 15. The sensor employs a symmetric van der Pauw disk of indium antimonide with an embedded gold inhomogeneity. The sensor does not contain any magnetic material. The magnetoresistance results from the field-dependent deflection of the current around the inhomogeneity. To understand the operation of the sensor it is necessary to consider the conductivity tensor. The elements of the tensor are

$$\begin{aligned} \sigma_{xx}(\beta) &= \sigma_{yy}(\beta) = \sigma/(1 + \beta^2), & \sigma_{zz}(\beta) &= \sigma \\ \sigma_{xy}(\beta) &= -\sigma_{yx}(\beta) = -\sigma\beta/(1 + \beta^2) \end{aligned} \quad (2)$$

where  $\beta = \mu H$  and  $\sigma$  is the conductivity of indium antimonide. The other tensor elements are zero. At  $H = 0$ , the conductivity tensor is just  $\sigma$  times the unity matrix. At large values of  $H$ , the off-diagonal elements dominate and the current is perpendicular to the applied field. Thus, the device has a low impedance at low fields and a high impedance at high fields. As can be seen from Fig. 15, the magnetoresistance is a strong function of the geometric parameter  $\alpha = r_a/r_b$  where  $r_a$  and  $r_b$  are the radius of the gold and indium antimonide, respectively. The sensor's

magnetoresistance is only weakly temperature dependent. Modeling results [47] indicate extraordinary magnetoresistance read heads might be useful for increasing magnetic storage density to 1 Tbit/in<sup>2</sup>. The SNR goes as the square root of sample volume. A disadvantage of the sensor is that it requires a significant biasing field.

e) *Ballistic magnetoresistance*: Ballistic magnetoresistance, a subject that has drawn considerable interest, involves a very small metallic contact between two ferromagnets. If the contact is small enough and there is no domain wall in the contact, electrons can pass ballistically between the two ferromagnets. The proposed mechanism [48], [49] for magnetoresistance involves nonadiabatic spin scattering across atomic scale magnetic domain walls trapped at the constriction. Values of magnetoresistance of several hundred percent [50] at room temperature, or even larger [51], have been reported in electrodeposited Ni-Ni nano-contacts 10–30 nm in diameter, but others have not been able to reproduce the results [52].

6) *Spin-Valve Transistors*: Spin-valve transistors [53] are spin-valves sandwiched between a pair of semiconductors, one of which is the emitter and the other the collector. The current through the device changes as a function of magnetic field. Current changes with increasing magnetic field as large as 200% have been observed, but, at present, the output currents are of order microamps and are too small for most sensor applications.

7) *Giant Magnetoimpedance (GMI) Magnetic Sensors*: The impedance of amorphous wires and ribbons decreases sharply [54], [55] in fields less than 50 Oe. The effect has been called the giant magnetoimpedance (GMI) effect. The impedance is a strong function of both the magnetic field and the frequency of the drive current. For uniform, single-phase materials, the origin of the effect is the impedance dependence of the skin depth, which is a function of the transverse permeability [56]. For NiFe/Cu composite wires, the magnitude of the impedance change peaks at a frequency of several MHz that depends on the annealing treatment of the wire. To use the effect requires using GHz drive currents.

8) *Magnetodiode*: A magnetodiode is essentially a semiconductor diode, or *pn* junction. In a magnetodiode, however, the *p* region is separated from the *n* region by an area of undoped silicon. The device is fabricated by depositing silicon and then silicon dioxide on a sapphire substrate. If a metal contact on the *p*-doped region is given a positive potential and a metal contact on the *n*-doped region is given a negative potential, holes in the *p*-type material and electrons in the *n*-type material will be injected into the undoped silicon. The current is the sum of the hole current and the electron current.

Some of the carriers, particularly those near the interface between the silicon and the silicon dioxide or near the interface between the silicon and the sapphire, will recombine. The loss of charge carriers increases the resistance of the material. In the absence of a field, recombination at both interfaces contributes to the resistance. A magnetic field perpendicular to the direction of travel of the charge carriers deflects them either down or up, depending on the direction of the field. Both holes and electrons are deflected in the same direction because they are traveling in opposite directions. Charge carriers near the interface between

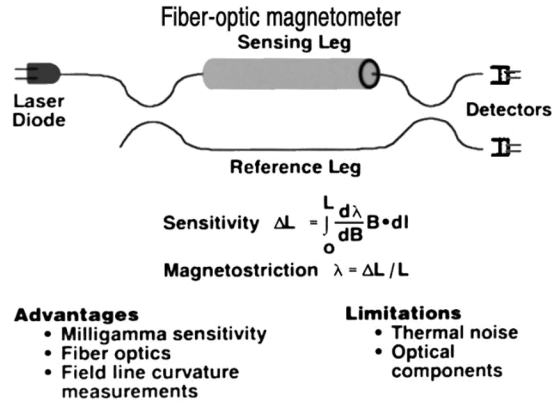


Fig. 16. Fiber-optic magnetometer using magnetostrictive material.

the silicon and the sapphire have a greater tendency to recombine than those near the interface between the silicon and the silicon dioxide. Thus, if the magnetic field deflects the charge carriers down, the resistance of the material is increased; if it deflects them up, the resistance is decreased. The response of a magnetodiode to a magnetic field is about ten times larger than the response of a silicon Hall-effect device.

9) *Magnetotransistor*: This sensor, like the magnetodiode, is an integrated silicon device. If the magnetodiode is a version of a *pn* junction, the magnetotransistor is a version of an *npn* transistor. Like the transistor, it consists of an *n*-doped emitter separated from a *n*-doped collector by a *p*-doped base. The difference is that there are two collectors instead of one. In the absence of a magnetic field, equal numbers of charge carriers arrive at both collectors. If there is a magnetic field perpendicular to the direction of travel of the charge carriers, they are deflected toward one collector or the other, depending on the direction of the field. The two-collector voltages are fed to a difference amplifier, whose output is proportional to the applied magnetic field.

Two different effects are used in magnetotransistors to detect magnetic fields. These are the Hall and Suhl effects. In the Hall effect, as described previously, the Lorentz force is compensated by an opposing electric field, which is sensed between the two collectors. The Suhl effect takes place when the Lorentz force is not compensated. An external magnetic field causes a change in trajectory of the moving carriers, resulting in a variation in the current distributions that is detected between the collector outputs. Although both effects occur simultaneously, it is possible to design devices in which one effect is dominant. The magnetotransistor is expected to be 100 times more sensitive than the silicon Hall-effect device and is based on a standard fabrication technology (i.e., silicon substrates).

#### 10) *Magnetostrictive Magnetometers*:

a) *Fiber-optic magnetometer*: The fiber-optic magnetometer employs two glass fibers that are arranged to form a Mach-Zender interferometer. As shown in the schematic, Fig. 16, light from a laser passes through a beam splitter into the two fibers, travels along the length of the fibers, is recombined, and arrives at a photodetector at the end of each fiber. One of the fibers is either wrapped around or coated with a magnetostrictive material, a material whose dimensions depend

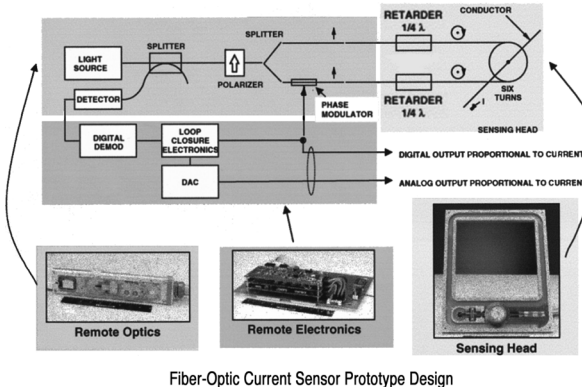


Fig. 17. Prototype design of a fiber-optic current sensor.

on the direction and magnitude of its magnetization. When the magnetostrictive material is magnetized by an external field, the length of the fiber changes. Because of the length change, the light traveling through the fiber arrives at the detector slightly out of phase with the light arriving from the reference fiber. The interference of the two light beams causes the light level at the photodetector to change by an amount dependent on the phase difference.

Changes in path length as small as  $10^{-13}$  m have been detected with this type of interferometer. The device is also uniquely sensitive to the orientation of field lines and could be employed to measure the curvature of the field lines as well as the strength of the magnetic field. Electroplating magnetostrictive materials onto fibers has been demonstrated.

The fiber-optic magnetometer has a sensitivity range of  $10^{-7}$  to  $10^{-2}$  G or  $10^6$  to  $10^6$  nT. It can be employed to sense either constant fields or fields fluctuating with frequencies below 60 kHz. A typical sensor is roughly 4 in long and 1 in wide. Fig. 17 shows a prototype design.

*b) Magnetolectric sensor:* Another interesting method for measuring the vector components of the magnetic field is to use laminates of magnetostrictive and piezoelectric materials. Dong *et al.* [57] used a three layer laminate consisting of two layers of a magnetostrictive material TERFENOL-D that surround a piezoelectric,  $\text{Pb}(\text{Mg}_{1/3}\text{Nb}_{2/3})\text{O}_3 - \text{PbTiO}_3$ , to fabricate a magnetoelectric sensor that has the potential to detect changes in the pT range. The length change induced in the magnetostrictive material by the magnetic field is converted into a voltage in the piezoelectric material. Thus, the device requires no energy to generate this voltage. Because the response at low fields is nonlinear, it is necessary to bias the device with a DC field of order 100 or more Oe. It is desirable to reduce the magnitude of this required field.

*11) Magnetooptical Sensor:* The magnetooptical sensor exploits another phenomenon discovered by Faraday. The Faraday effect involves the rotation of the plane of polarized light when traveling through a magnetic material. The effect is largest in a few crystals when the propagation directions of the light, the crystal axis, and the applied magnetic field are all aligned. To understand the Faraday polarization effect, we should consider that polarized light is composed of two

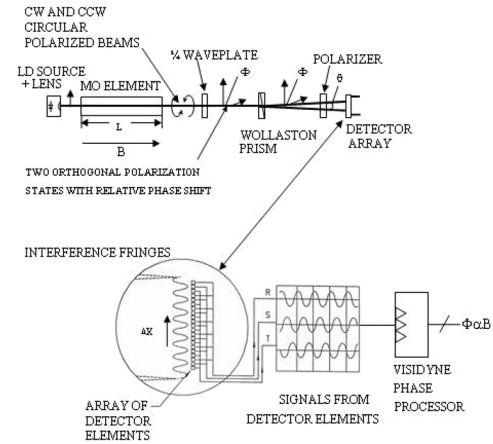


Fig. 18. Operation of magnetooptic magnetometer based on the interference of two optical beams one of which passes through the magnetooptic materials YIG. Courtesy of Visidyne Burlington, MA.

circularly polarized waves—one clockwise (CW) and one counterclockwise (CCW). The rotation of the plane of polarization occurs because of a change in the relative phases of the CW and CCW waves. More specifically, the Faraday effect results from the fact that the crystal's index of refraction is different if the electrons precess about the longitudinal magnetic field in the same or the opposite sense as the rotation of the electric field of the circularly polarized light. A figure of merit used to compare this effect between materials is the Verdet constant  $V$ , which has units of angular rotation per unit of applied field per unit of material length. In Fig. 18, there is a phase difference between the two circularly polarized beams after they pass through the magnetooptic material (MO) that is given by  $2BVL$  where  $L$  is optical path length in the MO. The phase difference gives rise to interference fringes in the detector array which can be measured with high sensitivity. It is possible to construct lab top magnetooptical magnetometers with a sensitivity of 30 pT.

A common magnetooptic material for field sensing is terbium gallium garnet, which has a Verdet constant of 0.5 min/(G cm). Along with a relatively high Verdet constant, this material also can take on a permanent magnetization. Because of this unique combination of magnetic characteristics, this material also has applications in magnetooptical memories.

The unique advantage that the magnetooptical sensor has over other magnetic sensors is its very fast response time. Sensors with gigahertz response have been fabricated.

*12) MEMS Based Magnetometers:* Many of the earliest designs of magnetic sensors utilized simple magnetic attraction to ferrous objects. The resulting motion was then measured to record or detect metal objects. A structure similar to a compass needle was the first magnetic field triggered fuze for mines. With the development of microelectromechanical systems (MEMS), the idea of using movement to sense magnetic fields is being reexamined.

Fabricating these devices has turned out to be challenging. This is especially true if the fabrication process requires using different technologies that are not naturally compatible. For example, the use of HF, often required to perform the release step

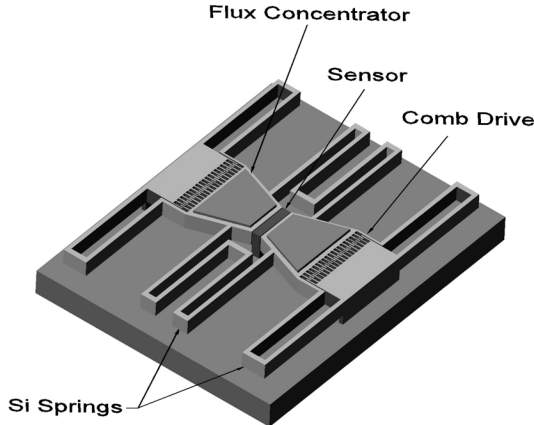


Fig. 19. Picture showing the concept of the MEMS flux concentrator. Note that there is a space between the substrate and the flux concentrators on the MEMS flaps.

needed to fabricate the MEMS structure, can damage other parts of the sensor.

Most of these sensors use the Lorentz force. An example of this is a magnetometer based on detecting the motion of a miniature bar magnet [58]. The hard magnetic material used was deposited by electrodeposition. The choice of materials for the hard magnet was limited by the need to use HF in the release step. The bar magnetic responds to the field without drawing any power. Fields as small as 200 nT have been detected optically. A similar approach was employed by DiLella *et al.* [59] who also use the rotation of a MEMS structure containing a permanent magnet. In this case, the field is determined by measuring the feedback required to maintain a constant tunneling current. They achieved a resolution of  $0.3 \text{ nT}/\sqrt{\text{Hz}}$  at 1 Hz. The sensitivity was limited by air pressure fluctuations. An alternative approach uses a xylophone resonator [60], [61]. In this approach, an AC current whose frequency is adjusted to be equal to the resonant frequency  $f_o$  of a MEMS beam is sent through the length of the beam. A DC field applied perpendicular to the axis of the beam will energize motion of the beam at the frequency  $f_o$ . The amplitude of the motion, that can be detected optically, is proportional to the field.

MEMS technology can improve magnetic sensors by minimizing the effect of  $1/f$  noise. The concept for a device that can accomplish this, the MEMS flux concentrator [7], [8], is shown in Fig. 19. In the device, the flux concentrators composed of soft magnetic material, are placed on MEMS flaps. The flux concentrators enhance the field. Decreasing the separation between the flaps increases the enhancement. The two MEMS flaps are forced to oscillate by applying an AC voltage to the electrostatic comb drives. By tuning the frequency, one can excite the normal mode in which the distance between the flaps oscillates. The resonant frequency for the MEMS structure is designed to be about 10 kHz. The oscillation of the MEMS flaps modulates the field at the position of the sensor and, hence, shifts the operating frequency of the sensor above the frequency where  $1/f$  noise dominates. Depending on the type of magnetic sensor used, this shift in operating frequency should increase the sensitivity of magnetometers by one to three orders of magnitude.

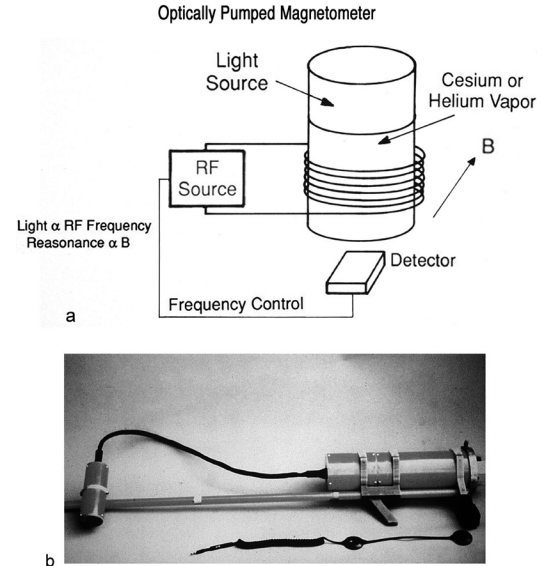


Fig. 20. Optically pumped magnetometer: (a) schematic; (b) example of hardware.

### B. Total Field Magnetometers

Total field magnetometers have the important advantage of insensitivity to rotational vibrations. Total field magnetometers use the fact that the splitting between some electron or nuclear spin energy levels is proportional to the magnitude of the magnetic field over a field range sufficient for magnetometry. Obtaining high sensitivity requires using resonances with narrow lines with long lifetimes. Such lines limit the sampling frequency. Thus, the sensitivity of these magnetometers decreases rapidly for frequencies above 10 Hz.

1) *Optically Pumped Magnetometer*: The optically pumped magnetometer illustrated in Fig. 20(a) is based on the Zeeman effect. In 1896, the Dutch physicist Zeeman showed that some of the characteristic spectral lines of atoms are split when the atoms are placed in a magnetic field; one spectral line becomes a group of lines with slightly different wavelengths. The splitting is particularly pronounced in alkali elements such as cesium and rubidium.

The optically pumped magnetometer exploits three energy states available to cesium's single valence electron: two lower states that are close together and one state at a much higher energy. The energy difference between the lower states corresponds to a radio-frequency spectral line or a microwave frequency, and the transition between one of the lower energy states and the higher state corresponds to a spectral line in the optical region.

The energy difference between the two lower states is due to a difference in the orientation of the spin axes of the electrons. An electron's spin axis can have only one of two orientations with respect to an external magnetic field, parallel or anti parallel, and one requires less energy than the other. The lower energy states are said to differ in one quantum unit of spin angular momentum. The higher state is a special one chosen because it has the same angular momentum as one of the lower states.

Consider a cesium vapor optically pumped with circularly polarized light. The amount of light the vapor is absorbing is monitored with a photodetector. Initially, some of the electrons in the vapor will be in one of the lower energy states and some in the other. When atoms absorb photons from circularly polarized light, their angular momentum necessarily changes by one unit. Thus, electrons in the energy state that differs from the higher state by one unit of angular momentum will absorb photons, but those in the energy state that has the same angular momentum as the higher state will not. Because some photons are absorbed, the beam of light is dimmed. An electron in the higher state drops down to one of the two lower states almost immediately. Each time an electron makes this transition, there is some probability that it will drop back to the state that cannot absorb light. Given enough time, nearly all of the electrons will end up there. The vapor, which is then said to be completely pumped, is relatively transparent to light.

If a radio-frequency field at the correct frequency is then applied parallel to the light path, it will flip the electrons over, changing their spin angular momentum. In effect, the radio-frequency field causes electrons to shuttle from one of the lower energy states to the other, undoing the optical pumping. As a result, the vapor again absorbs light. The radio frequency and optical effects combine to give a particularly sharp resonance, and it is this resonance the optically pumped magnetometer exploits.

The energy required to flip the electron spins, and, thus, the radio frequency, depends on the magnitude of the magnetic field. In the magnetometer, a feedback loop controls the radio frequency to maintain the minimum light transmission. The frequency, thus, serves as a measure of the magnetic field. The optically pumped magnetometer measures the total magnetic field, whatever its orientation, unlike most magnetometers, which measure only the component of the magnetic field that lies along the sensitive axis.

The sensitivity and dynamic range of the optically pumped magnetometer, like those of most magnetometers, are determined by the readout electronics. Typical sensitivities for cesium and helium vapor sensors, which is sometimes employed instead of cesium, are 700 kHz/G and 2.8 MHz/G, respectively. Optically pumped magnetometers have a sensitivity range of  $10^{-8}$  to 1 G or  $10^{-3}$  to  $10^5$  nT. This sensor, however, is relatively large, expensive and its power consumption is high (several watts). The sensitivity is high because the absorption lines are narrow due to the long relaxation times of the spins. Unfortunately, these long relaxation times limit the frequency response. Another difficulty is that the signal becomes very small when the field is oriented in some directions called dead zones. This difficulty is overcome by using several sensors with different orientations for their light-pumping beams. The cells holding the vapor cannot be too small because collisions with the cell walls limit the spin lifetime. This problem can be mitigated by using a buffer gas. A problem with using He is that it tends to diffuse through the cell walls.

An important property of this sensor is that the magnetic signature of the sensor itself can be made to be very low. One product that exploits this feature is a diver-held magnetometer, shown in Fig. 20(b), that is used for underwater mine

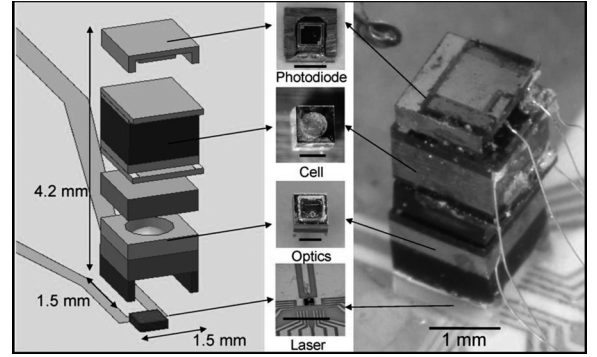


Fig. 21. Picture of the chip-scale atomic magnetometer that shows the stack of elements needed to make it operate. The cell is filled with Cs and a buffer gas.

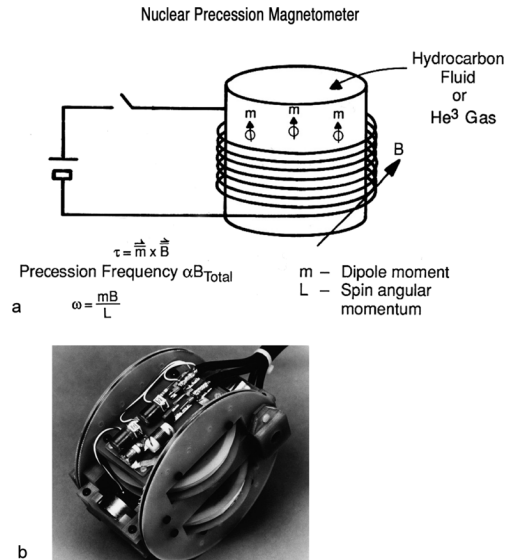


Fig. 22. Nuclear precession magnetometer: (a) schematic; (b) example of hardware.

field clearing. Several reviews have been written on optically pumped magnetometers [62], [63]. By eliminating spin-exchange relaxation using high K density and low magnetic fields a sensitivity of  $10 \text{ fT}$  or  $10^{-5} \text{ nT Hz}^{-1/2}$  was achieved in an optically pumped magnetometer [64].

At present, these sensors are limited by the cost and size of the glass containers holding the alkali gas. There are efforts to build glass ampoules into silicon chips. Fig. 21 shows an example [65] of a chip-scale atomic magnetometer fabricated using this approach. The fabrication process is nontrivial. Considerable work is required to make these lab units into stable units that can be used in the field. Though these “chip-scale atomic magnetometers” may never reach the sensitivity of the best current optically pumped magnetometers, they are much smaller and have the potential to be much lower in cost and energy consumption.

2) *Nuclear-Precession Magnetometer*: The magnetometer, illustrated in Fig. 22(a), exploits the response to a magnetic field of the nuclear moments of atoms in a hydrocarbon fluid such as benzene. The scale of atomic and nuclear moments is set by the Bohr magneton  $eh/2\pi m$  where  $e$  is the electronic charge,  $h$  is Planck's constant, and  $m$  is the mass. Since nuclei have masses

TABLE I  
CATEGORIES OF MAGNETIC SENSOR APPLICATIONS

<b>10<sup>-5</sup> G</b>	<b>1 G</b>	<b>10<sup>-5</sup> G</b>
<b>Category 3 High Sensitivity</b>	<b>Category 2 Medium Sensitivity</b>	<b>Category 1 Low Sensitivity</b>
<b>Definition</b> <ul style="list-style-type: none"> <li>• Measuring field gradients or differences due to induced (in Earth's field) or permanent dipole moments</li> </ul>	<b>Definition</b> <ul style="list-style-type: none"> <li>• Measuring perturbations in the magnitudes and/or direction of Earth's field due to induced or permanent dipoles</li> </ul>	<b>Definition</b> <ul style="list-style-type: none"> <li>• Measuring fields stronger than Earth's magnetic field</li> </ul>
<b>Major Applications</b> <ul style="list-style-type: none"> <li>• Brain function mapping</li> <li>• Magnetic anomaly detection</li> </ul>	<b>Major Applications</b> <ul style="list-style-type: none"> <li>• Magnetic compass</li> <li>• Munitions fuzing</li> <li>• Mineral prospecting</li> <li>• Traffic control</li> </ul>	<b>Major Applications</b> <ul style="list-style-type: none"> <li>• Noncontact switching</li> <li>• Current measurement</li> <li>• Magnetic memory readout</li> </ul>
<b>Most Common Sensor</b> <ul style="list-style-type: none"> <li>• SQUID gradiometer</li> <li>• Optically pumped magnetometer</li> </ul>	<b>Most Common Sensor</b> <ul style="list-style-type: none"> <li>• Search-coil magnetometer</li> <li>• Flux-gate magnetometer</li> <li>• Magnetoresistive magnetometer</li> </ul>	<b>Most Common Sensor</b> <ul style="list-style-type: none"> <li>• Search-coil magnetometer</li> <li>• Hall-effect sensor</li> <li>• Magnetoresistive magnetometer</li> </ul>

that are much larger than the electron's mass, nuclear magnetic moments are much smaller than electronic moments.

The protons in a fluid can be temporarily aligned by the uniform magnetic field created by a current through a coil. When the polarizing current is switched off, the protons will begin to precess about the ambient magnetic field. The spin axis of a proton that is out of alignment with a constant magnetic field, like the axis of a gyroscope out of alignment with a gravitational field, traces a circle about a line parallel to the field. The rate at which this circle is traced, called the precession frequency, is proportional to the strength of the magnetic field. Thus, the precessing protons generate a signal in the coil whose frequency is proportional to the strength of the magnetic field. Like the optically pumped magnetometer, the nuclear-precession magnetometer measures the total magnetic field. These magnetometers have a sensitivity range of  $10^{-6}$  to 1 G or  $10^{-1}$  to  $10^5$  nT. Their frequency range is limited by the gating frequency of the hydrocarbon fluid. A photo of this sensor is shown in Fig. 22(b).

Optical pumping of nuclear spins can be used in magnetometry. A gas of the isotope of helium, He<sup>3</sup>, is optically pumped, and then the precession frequency of the atomic nuclei is recorded with pickup coils. Because of the very long relaxation time, it only requires power during the short time when the spins are excited. This sensor has the potential for very high sensitivity ( $10^{-8}$  G or  $10^{-3}$  nT) with modest operating power (less than 0.5 W).

3) *Overhauser Magnetometer*: Overhauser magnetometers use an effect predicted [66], [67] by Overhauser when he was a graduate student at Berkeley in the 1950s. He predicted that in some systems you can get a factor of 1000 increase in the nuclear polarization by saturating the electron spin resonance. This increase occurs because the proton spins and electron spins interact via the hyperfine term in the Hamiltonian. This term is proportional to the vector product of the electron spin and the nuclear spin. The substance used in Overhauser magnetometers is a liquid containing protons and free radicals. Free radicals

are molecules with unpaired electrons that have electron resonant line widths that are very narrow, about 1 Oe or  $10^5$  nT. The narrow line width allows one to saturate the electron resonance and, hence, increase the proton polarization without using much power. The magnetic field is determined by measuring the proton precession frequency which is proportional to the magnetic field. The increased proton polarization increases the signal strength. Overhauser magnetometers can achieve noise levels of 0.015 nT/rt Hz at 1 Hz. Overhauser magnetometers are an order of magnitude more sensitive than proton precession magnetometers and have no dead zones.

### III. MAGNETIC SENSOR APPLICATIONS

There are a multitude of magnetic sensor applications, many of which are encountered everyday. The first nonlaboratory use of a magnetic sensor is thought to be fuzing of sea mines during World War II. Today, not one automobile, computer, or factory could operate as efficiently without magnetic sensors. However, nearly all applications can be sorted into four basic categories. The distinction between the first three categories is determined by how the sensor is used in relation to the ever-present magnetic field of the Earth. The fourth category is medical/biological applications. Table I defines the first three categories and within each category lists major applications and some of the most common sensors employed. In these applications, the effect of the Earth's magnetic field, which varies from roughly 0.1 to 1 G or  $10^4$  to  $10^5$  nT, must be considered. This is the reason we use the Earth's field and its properties to define the boundary between these categories. Category 1 applications are for magnetic fields greater than the Earth's field. Category 1 contains mainly low-sensitivity, industrial applications, for which the Earth's magnetic field is a background nuisance. We use the stability of the Earth's field to define the boundary between categories 2 and 3 applications. Because of solar, geological (i.e., Earth's molten core), and tidal effects, the Earth's magnetic field changes [4]. The

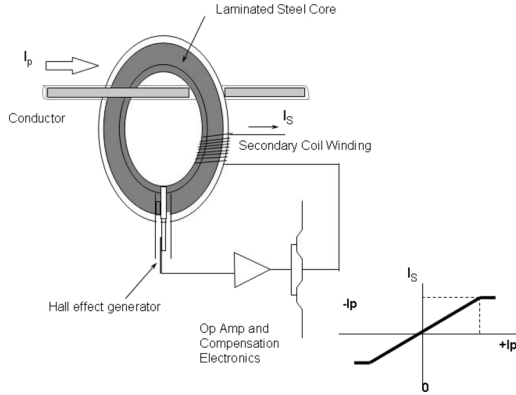


Fig. 23. Magnetic flux closed loop current sensor.

magnitude of the variations that range from as low as 1 part in 100 000 000 to as high as 1 part in 10 000 depends on the time of day, season, place and frequency. The fluctuations have a frequency dependence that is approximately  $1/f$ . For many applications in category 2, it is these variations in Earth's field that provide the performance-limiting noise.

In category 3 applications, one minimizes the effect of uncontrollable background magnetic noise source by using either a gradiometer or a finite differencing method. In a gradiometer, the sensor is designed so that this cancellation is done within the transduction mechanism. In a finite differencing method, two separate magnetometers with time-correlated signals are differenced. For either the gradient measurement or the finite difference method, the Earth's magnetic noise is considered to be coherent over the baseline of measurement. Thus, for this category, the performance-limiting issues arise from the sensor itself. Additional performance-limiting issues for finite differencing are the time correlation of the sensor outputs and the spatial coherence of Earth's field. For each category, specific applications will be further illustrated.

**Category 1. Low-Sensitivity Application: Current Sensing:** As an example of this category of sensor we will discuss the AC current sensor that is illustrated in Fig. 23. An AC current sensor produces a voltage output that is proportional to the current  $I_p$  passing through the sensor. The sensor responds like a resistor ( $V = IR$ ) in that the AC voltage is proportional to the AC current but the sensor offers complete electrical isolation. A closed loop technique using a magnetic core and feedback coil can be implemented to balance the magnetic flux from the current being sensed. This closed loop technique offers parts per million linearity and nanosecond response times for the sensor. The most common design uses a Hall Effect sensor mounted within a laminated magnetic core. The fact that the Hall sensor responds to the field perpendicular to its surface allows it to fit into a thin gap formed in the magnetic core.

An important design parameter of the current sensor is the permeability of the magnetic material used in the core. The permeability increases the flux density created by the current being sensed. However, because a gap is needed in the core to insert the magnetic sensor, most of this enhancement is lost. Fig. 24 shows an example of the magnetic gain achieved for various values of the magnetic permeability  $\mu$  of the core mate-

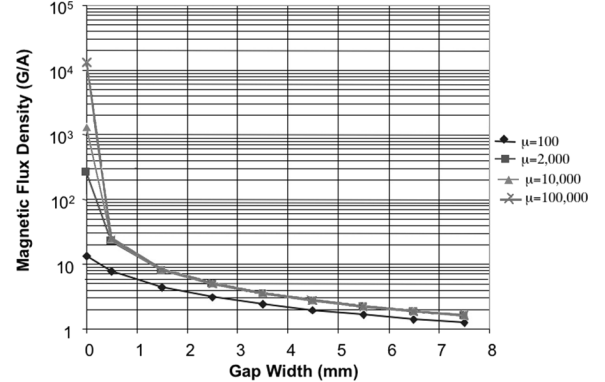


Fig. 24. Plot showing the magnetic response to an enclosed current for various values of the core permeability as a function of gap size.

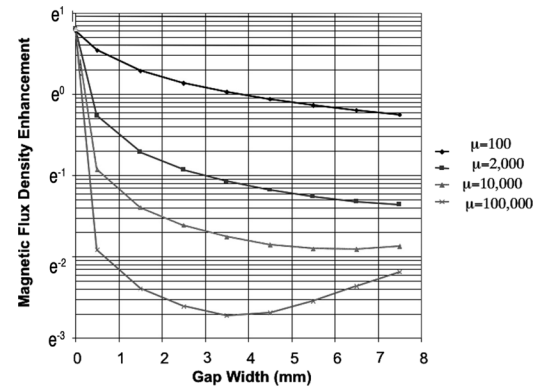


Fig. 25. Plot showing the magnetic response of a current sensor to an external field for various values of the core permeability as a function of gap size. Going from the top curve to the bottom curve corresponds to a monotonic increase in permeability.

rial as a function of the gap size. The effect of the gap greatly reduces much of the advantage of using high permeable material. One of the most important properties of a high performance current sensor is that it is insensitive to stray magnetic fields. Here, the permeability of the core is important for performance. Fig. 25 shows that external fields coming across the sensor are shunted away from going across the gap. Shielding attenuations of nearly 1000x can be achieved with highly permeable materials.

New designs using MR magnetic sensors are being introduced that significantly lower the sensor noise and offset drift. The unique symmetry in MR can be used to eliminate error due to offset and temperature drift. Fig. 26 shows performance data on a new closed loop current sensor that includes an MR sensor whose offset drift with temperature is reduced by a factor of 100.

**Category 2. Medium-Sensitivity Application: Magnetic Compassing:** Magnetic compassing involves determining the orientation of the sensor with respect to the Earth's magnetic field lines. The magnetic field measurements must be projected into the horizontal plane. This is often accomplished by either using a gimbal method that allows gravity to orient the sensors with a mechanical system or using tilt sensors and performing the orientation electronically [68]. For land navigation, pointing accuracies are also affected by magnetic anomalies such as mineral deposits and bridges.

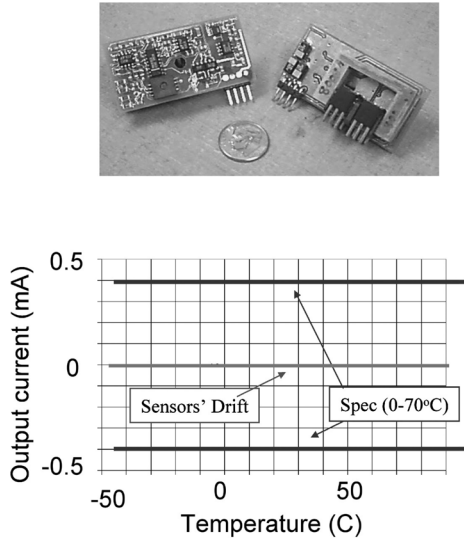


Fig. 26. Closed-loop current sensor that uses an MR sensor to achieve an ultra low offset temperature drift.

TABLE II  
THREE CATEGORIES OF COMPASSES

Application	Cost
1. Cardinal points (N, NW, W.....) 22° Accuracy (100 milligauss resolution) No tilt compensation Family anomaly compensation	\$1's
2. Heading/Orienteering 1° Accuracy (5 milligauss resolution)	\$10's
3. Navigation (<1% distance traveled) 0.1° Accuracy (0.5 milligauss resolution) Strap down (2-axis tilt measurement) 3-D calibration procedure	\$100's

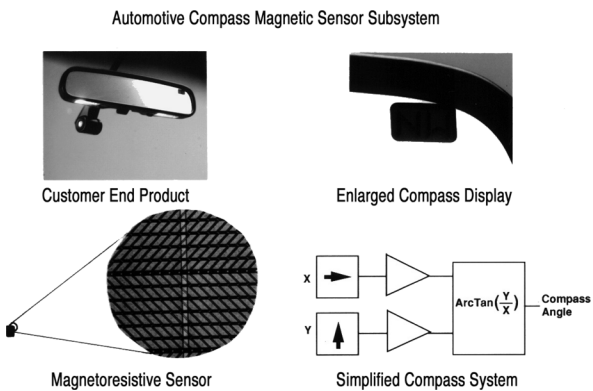


Fig. 27. Automotive rear-view mirror compass magnetic sensor system.

Table II shows the three general categories for using compasses. Cardinal points application is often used in moving vehicles to indicate the eight major heading directions. Fig. 27 illustrates this application in an automotive rear view mirror. In this type of compass, the accuracy is not better than 22.5° and often tilt compensation can be ignored if the compass is kept within 10° of horizontal. The heading or orientation compass is sometimes called the "boy scout compass." It approaches an accuracy of 1° and often uses a pin gimbal or level indication

TABLE III  
COMPASS ERROR SOURCES

Type of Error	Equivalent Magnetic Perturbation
<b>Sensors</b>	
Bias offsets, all different Unequal scale factors	Permanent
Axis nonorthogonality	Induced
Gravity misalignments	Induced
Sensor noise	Induced
<b>Magnetic Environment</b>	None
Soft forms objects	Induced
Hard forms objects	Permanent
Stable electrical currents	Permanent
AC electrical currents	None
Transient electrical currents	None

that allows the user to assist in making compass readings when horizontal.

Magnetic heading has been a reliable measurement for navigation for many centuries. It forms the basis for aviation with airport runways named by their magnetic heading. However, using a magnetic compass to determine the magnetic heading has some challenges to achieve high accuracy. The first is developing magnetic field sensors that can measure field with absolute accuracy. The second is then developing calibration algorithms that can compensate the magnetic field measurements for local variations in Earth's magnetic field due to ferrous metals and electrical currents that are nearby.

The purpose of the calibration procedure is to "model" the perturbations in Earth's magnetic field where the compass sensors are mounted. These perturbations or anomalies result from effects that are completely independent of the compass itself; thus, the solution can only be achieved by measuring the compass readout against truth data as part of a calibration procedure. This is performed for aircraft at a compass rose site surveyed at an airport. Once the calibration is performed, it will retain its accuracy unless the magnetic environment of where the compass is mounted changes. Experience has shown that mounting the compass in wing tips or a vertical stabilizer minimizes the changing effects from magnetic anomaly changes.

The calibration procedure provides numerical coefficients that are used to determine the true magnetic heading by correcting for the bias of the local anomalies. There are two compensation coefficients, the induced and permanent coefficients, determined during the calibration procedure. The induced coefficient compensates for errors that have 180° symmetry. The permanent coefficient compensates for errors with 360° symmetry. A compensation algorithm then uses these coefficients as part of a real-time correction of magnetic sensor readings to give true Earth's field and magnetic azimuth (heading). Not only do these coefficients compensate for errors from soft and hard magnetic materials nearby but they also compensate for intrinsic errors in the compass itself. These errors are sensor offset, sensor drift, and mis-alignments between the magnetic sensor axis, as well as misalignments between the gravity determination and the magnetic sensor coordinate system. Table III lists the sources of error for both the sensors and the magnetic environment. The only two sources of error that the compensation algorithm cannot correct are sensor noise

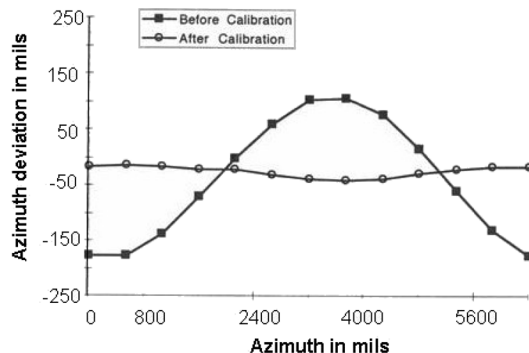


Fig. 28. Figure showing the improvement of an azimuthal sensor reading by using ISM calibration.

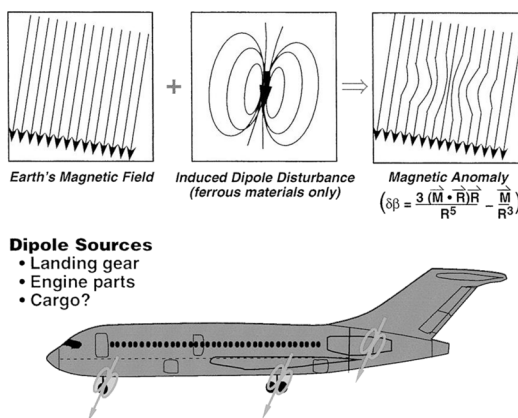


Fig. 29. Figure showing how an aircraft distorts the Earth's magnetic field lines and gives rise to a magnetic signature.

and anomalies due to transient electrical currents. Fig. 28 shows the improvement in compass accuracy that can be achieved with this coefficient compensation method. Sensors used in this application can achieve better than  $0.5^\circ$  accuracy.

**Category 3. High-Sensitivity Application: Magnetic Anomaly Detection:** A heavily researched magnetic sensor application is magnetic anomaly detection (MAD). This involves detecting at some distance away a ferromagnetic object (such as a mine, ship, tank, or aircraft). The dipole magnetic moment of ferromagnetic objects has two contributions. One is a permanent dipole moment. This acts like a bar magnetic in which the hard iron is magnetized. Typically, ships have “de-perming” procedures to reduce this effect. The second contribution is the induced magnetic dipole moment of the ferromagnetic material that is the response to the Earth’s magnetic field. The induced magnetic dipole is due to the magnetic permeability. If a material has a high magnetic permeability, it will perturb the ambient magnetic field. The total magnetic signature from a vessel or any other object is the superposition of these two contributions. Depending on the object and its past history either the permanent moment or the induced moment may dominate or the two moments may be comparable to one another. The effect of the two moments superimposes, as illustrated in Fig. 29 for an aircraft, to form what is called a magnetic depression in the ambient field.

The major advantages of magnetic sensing of objects are that the sensing technique is covert and nearly independent of weather conditions. Further, magnetic sensors can “see

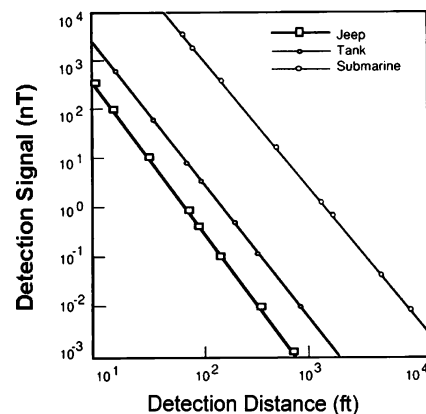


Fig. 30. Strength of the magnetic signal in nT detected from some military targets as a function of distance.

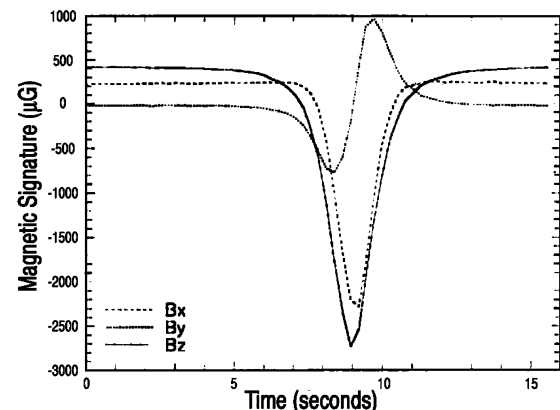


Fig. 31. Simple magnetic dipole vector signature from a compact ferromagnetic object, a Cat 950 front end loader.

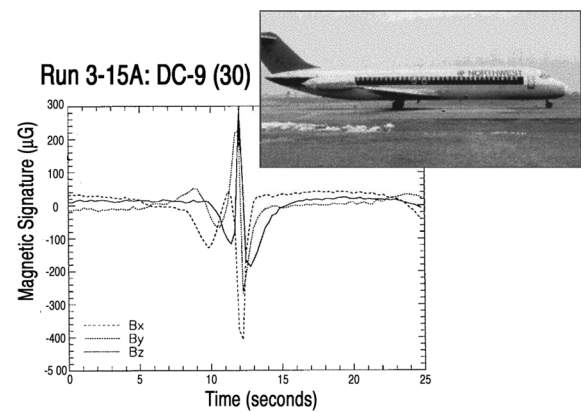


Fig. 32. Complicated vector signatures from a diffuse ferromagnetic object, a DC-9.

through” walls and foliage and it is nearly impossible to eliminate the signatures of ferromagnetic objects. A major factor in MAD is the detection range. Typical data exhibiting the  $1/r^3$  dipole field for a jeep, a tank, and a submarine are plotted in Fig. 30. The estimates of signal strength shown for the three targets are general approximations and do not represent specific versions of any target. As a ferrous object moves past a stationary magnetic sensor a signature can be recorded. Figs. 31 and 32 shows these magnetic vector component signatures for a

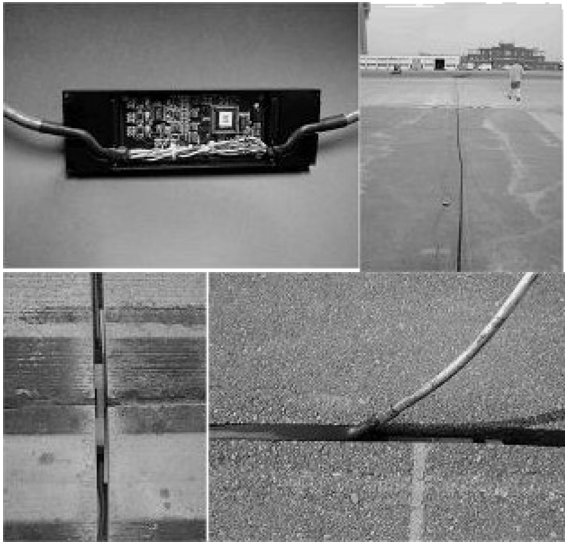


Fig. 33. Pictures showing the installation and use of magnetic sensors at a check-point.

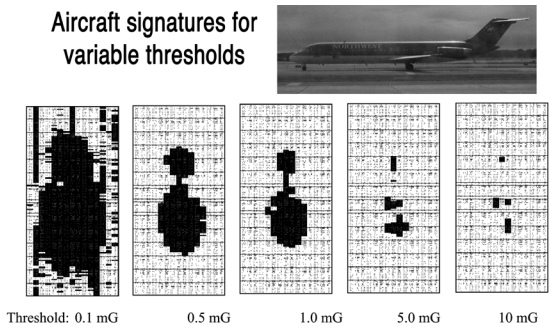


Fig. 34. Magnetic checkpoint: magnetic signature from a DC9-31 at different threshold detection levels.

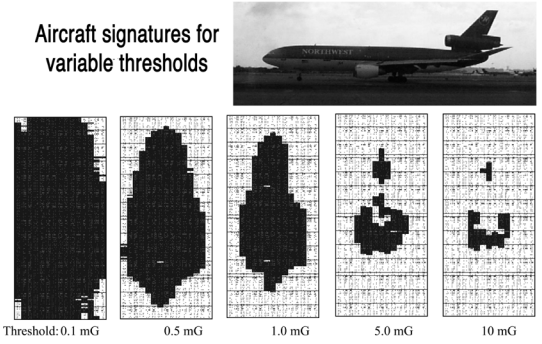


Fig. 35. Magnetic checkpoint: magnetic signature from a DC10-40 at different threshold detection levels.

compact ferrous object and an object containing ferromagnetic components that are more widely separated. We call the latter case a diffuse ferromagnetic object. One must be further from a diffuse ferromagnetic object for the signature to approach that of a dipole. The aircraft signature has more structure since each ferrous object on the plane contributes as a separate location for a magnetic disturbance. More information can be gained if an object moves past the magnetic sensors. Fig. 33 shows a system where a string of 16 magnetic sensors are embedded into a roadway. Figs. 34 and 35 show plots of data taken by this

sensor system for two types of aircraft. A threshold of total field strength is used at each data point to form a pattern signature of the aircraft. The peaks in the magnetic field disturbance can be identified with the gear and the outline of the aircraft.

An important consideration in MAD is the stability and uniformity of the Earth's magnetic field. In time-tracking a magnetic anomaly, it may not be possible to distinguish the anomaly from a time variation in the Earth's magnetic field. In general, there must be relative motion between the target and sensor for practical tracking of targets using only frequencies of 1 Hz or below. Relative motion is not required if one can detect AC currents or internal motion of ferromagnetic components in targets.

High sensitivity magnetometers are one of the important research tools used extensively in space exploration [69]. One of the special problems in this application is the need for a very large dynamic range. Another problem is that the spacecraft may not be magnetically clean. Thus, it is important to be able to remove the effect of magnetic fields due to the spacecraft.

**Category 4. Medical/Biological Applications:** Magnetic sensors can also be used for medical and biological applications. For example, magnetic tags can be attached to detect the presence of specific molecules. Magnetic microbeads were used as labels in a multianalyte biosensor to detect DNA hybridization on a micro-fabricated chip. The presence of the beads was detected by giant magnetoresistance (GMR) magnetoelectronic sensors embedded in the chip [70]. The motion of parts of the body such as the slight mechanical vibrations of eyelids or the articulatory movements of the tongue during speech [71] can also be measured using magnetic sensors. SQUIDS have been used to measure extremely weak magnetic fields generated by the brain [72] and in other medical tests [20]. Other workers have developed a prototype magnetic immunoassay system using a high temperature SQUID. The system measures liquid samples in an unshielded environment [73].

#### IV. SUMMARY AND FUTURE TRENDS

In this paper, most of the common magnetic sensing methods have been described and the underlying physical principles governing their operation have been highlighted. A varied set of applications that exploit specific characteristics of these sensors was also described.

The future trends in magnetic sensors should be discussed from these same two perspectives—physics and applications. In the past, discoveries of new physics phenomena have led to new sensor technologies. Many of the phenomena exploited by sensors were discovered in the 1800s and early 1900s (i.e., the Faraday effect, the Hall effect, superconductivity, etc.). However, as discussed here, there have been several more recent discoveries that have affected magnetic sensor technology. For example, Josephson tunneling in superconducting structures was observed in the 1960s. More recently, giant magnetoresistance and magnetic tunnel junctions have significantly affected information storage and sensor technology. It is likely that future discoveries will open new possibilities for improved magnetic sensors.

From an applications perspective, the need for improved sensors is ubiquitous. Magnetic sensors are used when other sensors have unwanted signals from the changing environment. The

trend is constantly toward smaller size, lower power consumption, and lower cost for similar or improved performance. There is not much need to improve the sensitivity independent of size, power, and cost. Instead, for each application, one needs to make a trade off between sensitivity, size, power, and cost. The possible routes for enhancing the performance of magnetic sensors are 1) new phenomenon, 2) new applications of existing phenomenon, 3) improved materials, and 4) improved processing and manufacturing. A major need is to reduce the cost of the signal processing electronics since, in many cases, the signal processing electronics is much more expensive than the sensor element.

There are, perhaps, more approaches to measuring magnetic fields than any other sensed parameter. Many of these approaches have gone through extensive engineering to the point where they are pushing the limits of physics. Thus, obtaining better material properties will be one of the major methods for making improvements in the size, power, and cost in magnetic sensors. Improvements in material properties are a result of the thousands of research studies published each year. Which materials will have the most significant improvement is hard to predict, and, most likely, in many cases, these improvements will come in minor steps.

There are, however, areas where large improvements are possible. For example, there has been research on half metals [74]. These are metals which have no minority spins states at the Fermi level. If MTJ sensors could be fabricated with materials that are half metals, the magnetoresistance would be infinite. It turns out to be difficult or impossible to produce materials that are half metals at room temperature. It is likely that the new field of spintronics will lead to improved magnetic sensors. A recent example of a new type of device is the spin-valve transistor described above [53].

#### ACKNOWLEDGMENT

The authors would like to thank the people who provided useful information for this review. They would also like to thank M. Miller and M. Tondra.

#### REFERENCES

- [1] J. E. Lenz, "A review of magnetic sensors," *Proc. IEEE*, vol. 78, no. 6, pp. 973–989, Jun. 1990.
- [2] A. E. Mahdi, L. Panina, and D. Mapps, "Some new horizons in magnetic sensing: high  $T_c$  SQUIDS, GMR, and GMI materials," *Sens. Actuators A*, vol. 105, pp. 271–285, 2003.
- [3] J. M. Daughton *et al.*, "Applications of spin dependent transport materials," *J. Phys. D*, vol. 22, pp. R169–R177, 1999.
- [4] W. H. Campbell, *Introduction to Geomagnetic Fields*. Cambridge, U.K.: Cambridge Univ. Press, 1997.
- [5] A. F. M. Nor *et al.*, "Noise in NiFeCo/Cu spin valve sensors," *Sens. Actuators A*, vol. 81, pp. 67–70, 2000.
- [6] R. J. M. v.d. Veerdonk *et al.*, "1/f noise in anisotropic and giant magnetoresistive elements," *J. Appl. Phys.*, vol. 82, pp. 6152–6164, 1997.
- [7] A. S. Edelstein and G. A. Fischer, "Minimizing 1/f noise in magnetic sensors using a microelectromechanical system flux concentrator," *J. Appl. Phys.*, vol. 91, pp. 7795–7797, 2002.
- [8] A. S. Edelstein *et al.*, "Progress toward a thousand-fold reduction in 1/f noise in magnetic sensors using an AC MEMS flux concentrator," *J. Appl. Phys.*, to be published.
- [9] P. Ripka, "Advances in fluxgate sensors," *Sensors and Actuators A*, vol. 106, pp. 8–14, 2003.
- [10] V. Pizzella *et al.*, "SQUID systems for biomagnetic imaging," *Supercond. Sci. Technol.*, vol. 14, pp. R79–R114, 2001.
- [11] R. Cantor, "SQUID's and emerging applications," *Supercond. Cryoelectron.*, vol. 13, pp. 16–22, 2001.
- [12] B. S. Deaver and W. M. Fairbank, "Experimental evidence for quantized flux in superconducting cyclinders," *Phys. Rev. Lett.*, vol. 7, pp. 43–46, 1961.
- [13] R. Doll and M. Näßauer, "Experimental proof of magnetic flux quantization in a superconducting ring," *Phys. Rev. Lett.*, vol. 7, pp. 51–52, 1961.
- [14] B. D. Josephson, "Possible new effects in superconductive tunneling," *Phys. Lett.*, vol. 1, pp. 251–253, 1962.
- [15] W. G. Jenks, S. S. H. Sadeghi, and J. P. Wikswo, Jr., "SQUIDS for non-destructive evaluation," *J. Phys. D: Appl. Phys.*, vol. 30, pp. 293–323, 1997.
- [16] J. G. Bednorz and K. A. Muller, "Possible high  $T_c$  superconductivity in the Ba-La-Cu-O system," *Z. Phys. B*, vol. 64, pp. 189–193, 1986.
- [17] M. K. Wu *et al.*, "Superconductivity at 93 K in a new mixed-phase Y-Ba-Cu-O compound system at ambient pressure," *Phys. Rev. Lett.*, vol. 58, pp. 908–910, 1987.
- [18] P. L. Richards, "Bolometric detectors for measurements of the cosmic microwave background," *J. Supercond.*, vol. 17, pp. 545–550, 2004.
- [19] H.-G. Meyer *et al.*, "SQUID technology for geophysical exploration," *Phys. Stat. Sol. C*, vol. 5, pp. 1504–1509, 2005.
- [20] R. Wakai, "Current and future technologies for biomagnetism," in *Proc. AIP Conf.*, 2004, vol. 724, pp. 14–19.
- [21] K. K. Berggren, "Quantum computing with superconductors," *Proc. IEEE*, vol. 92, no. 10, pp. 1630–1638, Oct. 2004.
- [22] M. G. Castellano *et al.*, "A new flux/phase qubit with integrated readout," *IEEE Trans. Appl. Supercond.*, vol. 15, no. 2, pp. 849–851, Jun. 2005.
- [23] T. Reich, T. Ortlepp, and F. H. Uhlmann, "Digital SQUID sensor based on SFQ technique," *IEEE Trans. Appl. Supercond.*, vol. 15, no. 2, pp. 304–307, Jun. 2005.
- [24] W. Meissner and R. Ochsenfeld, "Ein neuer effekt bei eintritt der supraleitfähigkeit," *Naturwissenschaften*, vol. 21, pp. 787–790, 1933.
- [25] M. Pannetier *et al.*, "Femtotesla magnetic field measurement with magnetoresistive sensors," *Science*, vol. 304, pp. 1648–1650, 2004.
- [26] R. S. Popovic, *Hall Effect Devices*. Bristol, U.K.: Inst. Physics, 2004.
- [27] S. Tumanski, *Thin Film Magnetoresistive Sensors*. Bristol, U.K.: Inst. Phys., 2001.
- [28] D. J. Mapps, "Magnetoresistive sensors," *Sens. Actuators A*, vol. 59, pp. 9–19, 1997.
- [29] T. R. McGuire, "Anisotropic magnetoresistance in ferromagnetic 3d alloys," *IEEE Trans. Magn.*, vol. 11, no. 4, pp. 1018–1038, Jul. 1975.
- [30] W. Y. Lee, M. F. Toney, and D. Mauri, "High magnetoresistance in sputtered Permalloy thin films through growth on seed layers of  $(\text{Ni}_{0.81}\text{Fe}_{0.19})_{1-x}\text{Cr}_x$ ," *IEEE Trans. Magn.*, vol. 36, no. 1, pp. 381–385, Jan. 2000.
- [31] M. N. Baibich *et al.*, "Giant magnetoresistance of (001)Fe/(001)Cr magnetic superlattices," *Phys. Rev. Lett.*, vol. 61, pp. 2472–2475, 1988.
- [32] G. Binasch *et al.*, "Enhanced magnetoresistance in layered magnetic structures with antiferromagnetic interlayer exchange," *Phys. Rev. B*, vol. 39, pp. 4828–4830, 1989.
- [33] P. P. Freitas *et al.*, "Spin valve sensors," *Sens. Actuators A*, vol. 81, pp. 2–8, 2000.
- [34] M. J. Carey *et al.*, "Spin valves using insulating cobalt ferrite exchange-spring pinning layers," *Appl. Phys. Lett.*, vol. 81, pp. 1044–1046, 2002.
- [35] K. Ounadjela *et al.*, "Interlayer magnetic coupling in Co/Ru/CoAg and Co/Cu/CoAg trilayer films: effect of Ag impurities on the exchange coupling," *J. Magn. Magn. Mater.*, vol. 156, pp. 267–268, 1996.
- [36] J. L. Leal and M. H. Kryder, "Interlayer coupling in spin valve structures," *IEEE Trans. Magn.*, vol. 32, no. 5, pp. 4642–4644, Sep. 1996.
- [37] J. S. Moodera *et al.*, "Large magnetoresistance at room temperature in ferromagnetic thin film tunnel junctions," *Phys. Rev. Lett.*, vol. 74, pp. 3273–3276, 1995.
- [38] E. Y. Tsymbal, O. N. Mryasov, and P. R. LeClair, "Spin-dependent tunnelling in magnetic tunnel junctions," *J. Phys.: Cond. Matter.*, vol. 15, pp. R109–R142, 2003.
- [39] M. Julliere, "Tunnelling between ferromagnetic films," *Phys. Lett. A*, vol. 54A, pp. 225–226, 1975.
- [40] S. S. P. Parkin *et al.*, "Giant tunnelling magnetoresistance at room temperature with MgO (100) tunnel barriers," *Nature Mater.*, vol. 3, pp. 862–867, 2004.
- [41] S. Yuasa *et al.*, "Giant room-temperature magnetoresistance in single-crystal Fe/MgO/Fe magnetic tunnel junctions," *Nature Mater.*, vol. 3, pp. 868–871, 2004.

- [42] W. H. Butler *et al.*, "Spin-dependent tunneling conductance of Fe|MgO|Fe sandwiches," *Phys. Rev. B*, vol. 63, pp. 054416/1–054416/12, 2001.
- [43] J. Mathon and A. Umerski, "Theory of tunneling magnetoresistance of an epitaxial Fe/MgO/Fe(001) junction," *Phys. Rev. B*, vol. 63, p. 220 403/1–4, 2001.
- [44] K. B. Klaassen, J. C. L. v. Peppen, and X. Xing, "Noise in magnetic tunnel junction devices," *J. Appl. Phys.*, vol. 93, pp. 8573–8575, 2003.
- [45] J.-B. Kammerer *et al.*, "A two-axis magnetometer using a single magnetic tunnel junction," *IEEE Sensors J.*, vol. 4, no. 3, pp. 313–321, Jun. 2004.
- [46] S. A. Solin *et al.*, "Enhanced room-temperature geometric magnetoresistance in inhomogeneous narrow-gap semiconductors," *Science*, vol. 289, pp. 1530–1532, 2000.
- [47] J. Moussa *et al.*, "Response of an extraordinary magnetoresistance read head to a magnetic bit," *J. Appl. Phys.*, vol. 94, pp. 1110–1114, 2003.
- [48] G. Tatara *et al.*, "Domain wall scattering explains 300% ballistic magnetoconductance of nanocontacts," *Phys. Rev. Lett.*, vol. 83, pp. 2030–2033, 1999.
- [49] C. A. Dartora and G. G. Cabrera, "Quantum transport properties of a two-channel atomic-sized magnetic contact," *Phys. Rev. B*, vol. 72, p. 064 456/1–064 456/19, 2005.
- [50] N. Garcia *et al.*, "Ballistic magnetoresistance in a magnetic nanometer sized contact: an effective gate for spintronics," *Appl. Phys. Lett.*, vol. 79, pp. 4550–4552, 2001.
- [51] H. D. Chopra and S. Z. Hua, "Ballistic magnetoresistance over 3000% in Ni nanocontacts at room temperature," *Phys. Rev. B*, vol. 66, pp. 020 403/1–020 403/3, 2002.
- [52] W. F. Egelhoff, Jr. *et al.*, "Artifacts in ballistic magnetoresistance measurements," *J. Appl. Phys.*, vol. 95, pp. 7554–7559, 2004.
- [53] O. M. J. v.t. Erve, "Transfer ratio of the spin-valve transistor," *Appl. Phys. Lett.*, vol. 80, pp. 3787–3789, 2002.
- [54] R. S. Beach and A. E. Berkowitz, "Giant magnetic field dependent impedance of amorphous FeCoSiB wire," *Appl. Phys. Lett.*, vol. 64, pp. 3652–3654, 1994.
- [55] X. P. Li *et al.*, "Enhancement of giant magnetoimpedance effect of electroplated NiFe/Cu composite wires by dc Joule annealing," *J. Appl. Phys.*, vol. 94, pp. 7626–7630, 2003.
- [56] S. Xiao *et al.*, "Giant magnetoimpedance and domain structure in FeCuNbSiB films and sandwiched films," *Phys. Rev. B*, vol. 61, pp. 5734–5739, 2000.
- [57] S. Dong, J.-F. Le, and D. Viehland, "Ultrahigh magnetic field sensitivity in laminates of TERFENOL-D and Pb(Mg<sub>1/3</sub>Nb<sub>2/3</sub>)O<sub>3</sub> – PbTiO<sub>3</sub> crystals," *Appl. Phys. Lett.*, vol. 83, pp. 2265–2267, 2003.
- [58] H. H. Yang *et al.*, "Ferromagnetic micromechanical magnetometer," *Sens. Actuators A*, vol. 97–98, pp. 88–97, 2002.
- [59] D. DiLella *et al.*, "A micromachined magnetic-field sensor based on an electron tunneling displacement transducer," *Sens. Actuators*, vol. 86, pp. 8–20, 2000.
- [60] R. B. Givens *et al.*, "A high sensitivity, wide dynamic range magnetometer designed on a xylophone resonator," *Appl. Phys. Lett.*, vol. 69, pp. 2755–2757, 1996.
- [61] D. K. Wickenden, "Polysilicon xylophone-bar magnetometers," in *Proc. Technical Digest Solid-State Sensor and Actuator Workshop*, Hilton Head Island, SC, 2000, pp. 150–153.
- [62] W. Happer, "Optical pumping," *Rev. Mod. Phys.*, vol. 44, pp. 169–249, 1972.
- [63] D. Budker, W. Gawlik, D. F. Kimball, S. M. Rochester, V. V. Yashchuk, and A. Weis, "Resonant nonlinear magneto-optical effects in atoms," *Rev. Mod. Phys.*, vol. 74, pp. 1153–1201, 2002.
- [64] J. C. Allred, R. N. Lyman, T. W. Kornack, and M. V. Romalis, "High-sensitivity atomic magnetometer unaffected by spin-exchange relaxation," *Phys. Rev. Lett.*, vol. 89, pp. 130 801/1–130 801/4, 2002.
- [65] P. D. D. Schwindt, S. Knappe, V. Shah, L. Hollberg, J. Kitching, L.-A. Liew, and J. Moreland, "Chip-scale atomic magnetometer," *Appl. Phys. Lett.*, vol. 85, pp. 6409–6411, 2004.
- [66] A. W. Overhauser, "Polarization of nuclei in metals," *Phys. Rev.*, vol. 91, pp. 476–476, 1953.
- [67] ———, "Polarization of nuclei in metals," *Phys. Rev.*, vol. 92, pp. 411–415, 1953.
- [68] G. J. Olson *et al.*, "Nongimballed solid-state compass," in *Technical Digest, Solid-State Sensor and Actuator Workshop*, Hilton Head Island, SC, 1994, pp. 197–200.
- [69] M. H. Acuna, "Space-based magnetometers," *Rev. Sci. Instrum.*, vol. 73, pp. 3717–3736, 2002.
- [70] M. M. Miller, P. E. Sheehan, R. L. Edelstein, C. R. Tamanaha, L. Zhong, S. Bounnak, L. J. Whitman, and R. J. Colton, "A DNA array sensor utilizing magnetic microbeads and magnetoelectronic detection," *J. Magn. Magn. Mater.*, vol. 225, pp. 138–144, 2001.
- [71] Y. Sonoda, "Applications of magnetometer sensors to observing bio-mechanical movements," *IEEE Trans. Magn.*, vol. 31, no. 2, pp. 1283–1290, Mar. 1995.
- [72] S. Masahiro, T. Hiroaki, K. Kunio, and H. Yasuhiro, MEGvision Magnetoencephalograph System and Its Applications 2004, vol. 38, pp. 23–27, Yokogawa Tech. Rep. (English Edition).
- [73] A. Tsukamoto *et al.*, "Development of multisample biological immunoassay system using HTSSQUID and magnetic nanoparticles," *IEEE Trans. Appl. Supercond.*, vol. 15, no. 2, pp. 656–659, Jun. 2005.
- [74] J.-H. Park *et al.*, "Direct evidence for a half-metallic ferromagnet," *Nature*, vol. 392, pp. 794–796, 1998.



**James Lenz** is an Adjunct Professor at the University of Minnesota, Minneapolis. He has broad experience in magnetics and magnetic sensing from aeromagnetic mapping to electromagnetic testing to position sensing and controls to compassing.



**Alan S. Edelstein** is the Team Leader in magnetic sensors at the Army Research Laboratory, Adelphi, MD. Though he has studied nanomaterials, most of his career has been devoted to investigations in various fields of magnetism. His major interests in magnetism are strongly correlated electrons systems and magnetic sensors and their applications.